People's Democratic Republic of Algeria Ministry of Higher Education and Scientific Research

Amar Thelidji University – Laghouat

FACULTE: TECHNOLOGY

DEPARTEMENT: PROCESS ENGINEERING

MASTER THESIS

Presented by:

MAIZI Abdeljalil

DOMAIN: Science and Technology

SECTOR: Process Engineering.

OPTION: Materials Engineering

Theme

Theoretical investigation of the structural, mechanical, and nonlinear optical properties of three cesium iodate polymorphs

Jury members:

First and last name	Grade	Quality
BOUTASSOUNA Nassima	MAA	President
BOUREZG Mohamed Tahar	MCB	Examiner
BELHADJ Soraya	MCB	Advisor

Academic year: 2025 - 2026

Dedication

We dedicate this modest work first and foremost to my beloved parents, who have never ceased making sacrifices for my well-being, happiness, and success, and who have always guided me on the right path in life. May God bless them and keep them for me.

To my brothers and my sister.

To my dear friends.

To all those who contributed, directly or indirectly, to the realization of this work.

Abdeldjalil MAIZI

Acknowledgments

First and foremost, we would like to thank Almighty Allah for granting us the strength, courage, and means to accomplish this work.

We would like to express our sincere gratitude to Dr. BELHADJ Soraya for his guidance, support, and supervision throughout this dissertation. Your valuable advice, encouragement, and trust enabled me to progress efficiently and confidently. Thank you for believing in me and for your continuous support.

We would also like to extend our heartfelt thanks to Dr. BOUTASSOUNA Nassima and Dr. BOUREZG Mohamed Tahar for accepting to evaluate this work. It is a great honor to have you as members of the dissertation jury.

And since this work was accomplished within the physics and chemistry of materials laboratory of AMAR THELIDJI University of LAGHOUAT we

would not like to miss the opportunity to thank the head of the laboratory; Pr. TAOUTI Mohamed Benabdallah.

And also, we do not forget to thank the head of GPM formation Pr. DJEDID Mebrouk and the head of process engineering department Mr. BENALIA Mokhtar.

We extend our sincere thanks to all the honorable professors of the process engineering department and to all our colleagues.

Finally, we would like to thank everyone who contributed, directly or indirectly, to the completion of this work.

List of abbreviations

Å: Angstrom

ABINIT: Ab Initio Simulation Package

AU: Universal Elastic Anisotropy Index

B: Bulk Modulus

BFGS: Broyden-Fletcher-Goldfarb-Shanno Optimization Method

C-$CsIO_3$: Cubic Cesium Iodate

CIF: Crystallographic Information File

C_{ij}: Elastic Constants Tensor Components

$CsIO_3$: Cesium Iodate

DFPT: Density Functional Perturbation Theory

DFT: Density Functional Theory

d_{ij}: Piezoelectric Coefficients

E: Young's Modulus

eV: Electron Volt

G: Shear Modulus

GGA: Generalized Gradient Approximation

GPa: Gigapascal

Ha: Hartree

IBZ: Irreducible Brillouin Zone

k-points: Reciprocal Space Sampling Points

LDA: Local Density Approximation

M-$CsIO_3$: Monoclinic Cesium Iodate

NLO: Nonlinear Optical

PP-PW: Pseudopotential Plane Wave

PW-LDA: Perdew–Wang Local Density Approximation

R-$CsIO_3$: Rhombohedral Cesium Iodate

r_{ij}: Electro-optic Coefficients

SHG: Second Harmonic Generation

VASP: Vienna Ab initio Simulation Package

σ: Poisson's Ratio

List of figures

	Number	Captions	Page
Chapter I	Figure I.1	Main families of materials	04
	Figure I.2	Simplified representation of an atom	06
	Figure I.3	Diagrams of band structures	08
	Figure I.4	Property value of metal materials	11
	Figure I.5	Property value of organic materials	11
	Figure I.6	Property value of mineral materials	11
	Figure I.7	Diagram of a two-dimensional network	12
	Figure I.8	Mesh construction	13
	Figure I.9	Theoretical diagram established according to the theory of energy bands indicating the position of the valence and conduction bands	14
	Figure I.10	Direct bandgap	16
	Figure I.11	Indirect bandgap	16
	Figure I.12	Wien2k code logo	19
	Figure I.13	Wien2k code structure	21
	Figure I.14	Origin Ver19 logo	22
Chapter II	Figure II.1	Monoclinic primitive cell of M-$CsIO_3$	27
	Figure II.2	Rhombohedral primitive cell of R-$CsIO_3$	27
	Figure II.3	Cubic primitive cell of C-$CsIO_3$	28
	Figure II.4	Environment of the iodine atom in iodate compounds	28
	Figure II.5	Structural optimization and equilibrium parameters of $CsIO_3$ polymorphs	30
	Figure II.6	Elastic constants (C_{ij}) of M-$CsIO_3$, R-$CsIO_3$, and C-$CsIO_3$	35
	Figure II.7	Mechanical parameters (B, G, E and B/G ratio) of $CsIO_3$ polymorphs	38
	Figure II.8	Bulk modulus B of M-$CsIO_3$ in 2D and 3D	42
	Figure II.9	Young's modulus E of M-$CsIO_3$ in 2D and 3D	42
	Figure II.10	Bulk modulus B of R-$CsIO_3$ in 2D and 3D	43
	Figure II.11	Young's modulus E of R-$CsIO_3$ in 2D and 3D	43
	Figure II.12	Bulk modulus B of C-$CsIO_3$ in 2D and 3D	44
	Figure II.13	Young's modulus E of C-$CsIO_3$ in 2D and 3D	44

List of tables

	Number	Captions	Page
Chapter I	Table I.1	Mass and electric charges of elementary particles	07
	Table I.2	Periodic classification of chemical elements principle	08
	Table I.3	Periodic classification of elements	09
	Table I.4	Definition of the crystallographic reference frame and characteristics of the seven crystal systems and fourteen Bravais lattices	13
Chapter II	Table II.1	Crystallographic data of M-$CsIO_3$, R-$CsIO_3$, and C-$CsIO_3$	26
	Table II.2	Computational parameters used in the calculations	31
	Table II.3	Optimized structural parameters of M-$CsIO_3$	32
	Table II.4	Optimized structural parameters of R-$CsIO_3$	32
	Table II.5	Optimized structural parameters of C-$CsIO_3$	33
	Table II.6	Elastic constants (Cij) of $CsIO_3$ polymorphs	36
	Table II.7	Mechanical properties (B, G, E, ν, B/G) of $CsIO_3$ polymorphs	38
	Table II.8	Elastic anisotropy indices of $CsIO_3$ polymorphs	41
	Table II.9	Piezoelectric coefficients d_{ij} (pC/N) calculated for M-$CsIO_3$ and R-$CsIO_3$	46

List of content

CONTENTS

General introduction 01

Chapter I: Bibliographic review

I.1. Introduction 03

I.2. Materials concepts 03

I.2.1. Materials choosing 03

I.2.2. Types of materials 03

I.2.2.1. Metallic materials 04

I.2.2.2. Organic materials 04

I.2.2.3. Mineral or inorganic materials 04

I.2.2.4. Composite materials 04

I.2.3. Materials properties 04

I.2.3.1. Physical properties 04

I.2.3.2. Mechanical properties 05

I.3. Classification 06

I.3.1. Classification of chemical elements 06

I.3.2. Classification of materials and properties 09

I.3.2.1. Main classes of materials 09

I.3.2.2. Usage properties 10

I.3.2.3. Principal properties of main materials classes 10

I.4. Crystalline solids 12

I.4.1. Crystal structure 12

I.5. Conductivity 14

I.5.1. Semiconductors 15

I.5.2. Direct gap and indirect gap 15

I.5.2.1. Direct band gap 15
I.5.2.2. Indirect band gap 16
I.5.3. Chemical bonds 16
I.5.3.1. Strong bonds 16
I.5.3.2. Weak bonds 17
I.6. Density functional theory (DFT) 17
I.6.1. Schrödinger equation 18
I.6.2. Hohenberg and Kohn theorems 18
I.6.3. Kohn-Sham theorem 19
I.6.4. Exchange-correlation potential 19
I.6.4.1. Local density approximation (LDA) 19
I.6.4.2. Generalized gradient approximation (GGA) 20
I.6.4.3. WC-GGA approximation 20
I.6.4.4. PBE-SOL approximation 20
I.6.4.5. TB-mBJ approximation 20
I.7. WIEN2k code 21
I.7.1. Main steps to follow in Wien2k code 22
I.7.1.1. Initialization 22
I.7.1.2. SCF calculation 22
I.7.1.3. Exploring material properties 23
I.8. Origin software 23
Conclusion 24
References 25

Chapter II: Calculations, results and discussion

II.1. Introduction 27
II.2. Calculation details and parameters 27
II.2.1. Methods adopted 27

II.2.1.1. Abinit code ……..27
II.2.2. Convergence step 28
II.2.3. Optimization step ……28
II.3. Structural study of the $CsIO_3$ polymorphs.....28
II.3.1. Historical ……29
II.3.2. Structural properties of cesium iodates 31
II.4. Elastic properties 32
II.4.1. Elastic constants 32
II.4.2. Other mechanical properties 36
II.4.3. Elastic anisotropy 41
II.5. Piezoelectric properties 45
II.6. Nonlinear optical properties 46
II.6.1. Electro-optical coefficients 46
II.6.2. Second order optical coefficients ……47
II.7. Conclusion 49
References 51
General conclusion 53

General introduction

General introduction

In recent decades, the rapid development of science and technology has led to an increasing demand for advanced materials with specific physical and chemical properties [1]. The continuous progress in electronics, photonics, and optical communication technologies has stimulated extensive research on functional materials that exhibit remarkable structural, mechanical, and optical performances [2].

Among these materials, iodate compounds have attracted considerable attention due to their interesting optical and nonlinear optical properties [3]. Cesium iodate ($CsIO_3$) is one of the most important iodate-based materials and can exist in different polymorphic forms. The variation in crystal structure may significantly influence its physical properties, making the study of its polymorphs essential for understanding their behavior and potential technological applications [4].

The development of computational methods based on Density Functional Theory (DFT) has provided powerful tools for investigating the properties of materials at the atomic scale. These theoretical approaches allow the prediction of structural, mechanical, electronic, and optical properties with high accuracy while reducing the need for expensive and time-consuming experimental procedures [5,6].

The objective of the present work is to investigate theoretically the structural, mechanical, piezoelectric, and nonlinear optical properties of cesium iodate polymorphs using first-principles calculations. Particular attention is paid to the influence of crystal symmetry on the stability and physical properties of the different phases.

Our work is organized as follows:

- General introduction.
- Chapter I: Bibliographic review.
- Chapter II: Calculations, results and discussion.
- General conclusion.

References

[1] W.D. Callister and D.G. Rethwisch, Materials Science and Engineering: An Introduction, 10th Edition, Wiley, 2018.

[2] B.E.A. Saleh and M.C. Teich, Fundamentals of Photonics, 3rd Edition, Wiley, 2019.

[3] D.S. Chemla and J. Zyss, Nonlinear Optical Properties of Organic Molecules and Crystals, Academic Press, 1987.

[4] X. Wang, M. Zhang, and G. Zhang, Recent advances in iodate-based nonlinear optical materials, Cryst. Eng. Comm., vol. 22, pp. 1234-1245, 2020.

[5] P. Hohenberg and W. Kohn, Inhomogeneous Electron Gas, Physical Review, vol. 136, pp. B864-B871, 1964.

[6] W. Kohn and L.J. Sham, Self-Consistent Equations Including Exchange and Correlation Effects, Physical Review, vol. 140, pp. A1133-A1138, 1965.

Chapter I:

Bibliographic search

I.1. Introduction

A wide variety of physical materials have been explored and utilized by humans, such as metals, insulators, superconductors, and semiconductors. These materials have significantly contributed to technological progress and improved daily life. In particular, semiconductors have played a crucial role in advancing physics and modern technology due to their outstanding and unique properties [1].

I.2. Materials concepts

I.2.1. Materials choosing

Materials are fundamental to technological and industrial development, as the success of any manufactured product strongly depends on the appropriate choice of materials. However, selecting a suitable material is not a straightforward task due to the wide range of available material families. In engineering design, the primary objective is often to reduce cost while satisfying required performance criteria.

The selection process typically starts with evaluating the properties and costs of candidate materials, and it can be facilitated by using material or performance indices related to the desired characteristics. For instance, superconducting materials exhibit zero electrical resistance, allowing electric current to persist indefinitely in a closed loop, which enables the generation of stable magnetic fields [2].

I.2.2. Types of materials

A material is of natural or artificial origin that men use and/or design to manufacture objects, construct buildings or machines.

Materials are differentiated according to their origin (from living beings for example) and their properties, whether mechanical (flexibility or rigidity, etc.), chemical (permeability or impermeability to water, etc.) or even physical (conductivity of the electricity or heat, etc.).

Materials are generally classified into different large families: metallic materials and organic materials

I.2.2.1. Metallic materials

Which include:

- Metals: iron, copper, bronze, etc.
- Metal alloys: stainless steel, etc.

I.2.2.2. Organic materials

Organic materials come from living beings, plants or animals (wood, cotton, paper, etc.).

I.2.2.3. Mineral or inorganic materials

For example: rock, ceramic, glass, etc.

I.2.2.4. Composite materials

Composite materials combine several materials from different families to obtain multiple properties (carbon fiber, etc.) [3].

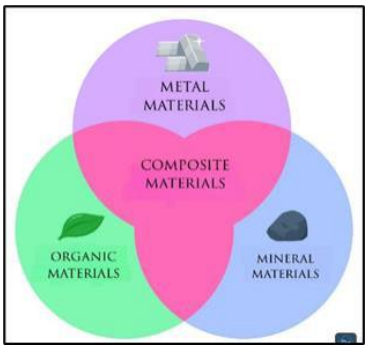


Figure I.1: Main families of materials [3].

I.2.3. Materials properties

I.2.3.1. Physical properties

Pure metals generally exhibit high electrical and thermal conductivity, as well as relatively high density. Among them, silver is considered the most efficient electrical conductor, with a conductivity of approximately 6.30×10^7 S/m, followed by copper, gold, and aluminum. In contrast, iron has a lower conductivity, and this property decreases further when impurities are introduced. For instance, low-carbon steel (such as 1010 steel containing about 0.10%

carbon) shows significantly reduced electrical conductivity compared to pure iron, which highlights the strong influence of impurities on the conductive behavior of metallic materials [4].

In general, metals tend to have higher densities than most non-metallic materials, although this property varies significantly from one metal to another. For example, lithium is one of the least dense metals, whereas osmium is among the densest known elements. Alkali and alkaline earth metals typically exhibit low density and relatively low hardness, and alkali metals are also characterized by low melting points. In contrast, many other metals possess high densities due to their closely packed crystal structures, which contribute to their compact atomic arrangement [5].

Metals are also generally characterized by good malleability and high ductility which allow them to deform without breaking. Thus, pure copper can be stretched to form electrical wires, pipes (plumbing), be plated and hammered into the shape of pans; Pure gold can also be formed into very thin sheets. Conversely, certain alloy elements make it possible to harden the metal: this is for example the case of carbon which hardens iron to give steel, tin which hardens copper to give family, at the refractory metals, because these elements have a large number of delocalized electrons in their structure. However, other factors also come into play, such as the atomic radius, the atomic number, the number of bonding orbitals, the superposition of the energies of the orbitals and the type of crystal structure; Centered cubic structures thus give weaker metallic bonds than face-centered cubic and compact hexagonal structures because the latter have a higher coordination, that is to say they bind more neighboring atoms than the first.

I.2.3.2. Mechanical properties

Hooke's law can model the elastic deformation of metals when the deformation is a linear function of the stress. The application of forces greater than the elastic limit or heating can lead to permanent deformation of the object, which corresponds to plastic deformation [6]. This irreversible modification of the arrangement of the atoms of the material can result from the application:

- A force or work in tension , compression, shearing, bending or torsion.
- Heating, which affects the mobility of structural defects in the material, such as

grain boundaries, vacancies, screw and corner dislocations, and stacking faults of crystalline and non-crystalline solids. The movement of such defects requires activation energy and is therefore limited by the atomic diffusion rate.

- Viscous flow around grain boundaries, for example, can give rise to creep or metal fatigue. It can also contribute to significant changes in microstructure, such as grain growth and localized increase in material density by elimination of intergranular porosity. Additionally, the non-directional nature of metal bonds could contribute significantly to the ductility of solid metals [7].

I.3. Classification

I.3.1. Classification of chemical elements

The atoms of chemical elements differ by their structure at the subatomic scale, that is to say the number and nature of the elementary particles, which constitute them:

- **Nucleus:** protons and possibly neutrons.
- **Electronic procession gravitating around the nucleus:** electrons in numbers equal to the protons in an atom in equilibrium [8].

The protons are positively charged and the electrons negatively, have equal elementary charges in absolute values, so that the atom is electrically neutral in the equilibrium state (figure I.2). The mass of the electron is negligible compared to that of the proton or neutron (table I.1).

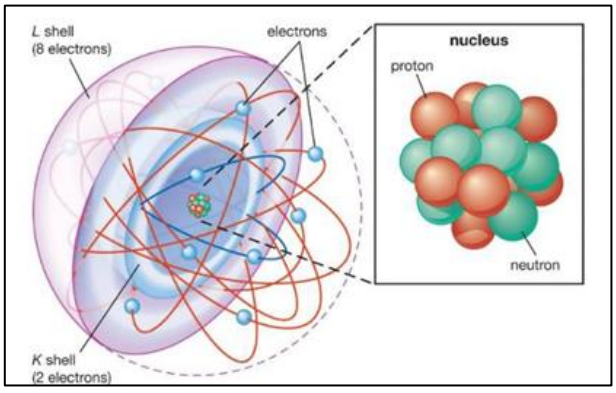


Figure I.2: Simplified representation of an atom [8].

The orbits of electrons occupy successive layers in an atom, corresponding to discrete energy levels, which become bands in solids grouping several atoms. These levels can only contain a limited number of electrons: two for the first, eight for the following levels (at least when they are in the external position), and forbidden bands separate them. We call the Fermi energy of the atom considered the upper limit of the filling of the electronic energy states at thermodynamic equilibrium and at absolute zero [9].

Table I.1: Mass and electric charges of elementary particles [9].

	Mass (kg)	Mass (amu)	Charge (relative)	Charge (C)
Proton	1.67262×10^{-27}	1.00727	+I	$+1.60218\times10^{-19}$
Neutron	1.67493×10^{-27}	1.00866	0	0
Electron	0.00091×10^{-27}	0.00055	-I	-1.60218×10^{-19}

In the periodic classification table of chemical elements; Mendeleev table (table I.2 and I.3); the lines or periods are the successive levels of the electronic layers. The columns or groups are the number of electrons in the outer layer.

From the second element of the fourth period (calcium), the internal electronic layers can receive more than eight electrons so additional elements are intercalated before moving to the next group. The chemical properties of an element come essentially from its electrons, and in particular those in the outer layer, called valence electrons, these properties are therefore linked to the group (column of the periodic table) to which it belongs.

- **Isotopes:** Elements with the same atomic number (and therefore the same electronic and chemical properties), but different atomic masses, due to a different number of neutrons. In nature, some chemical elements exist as mixtures of isotopes; this results in non-integer average atomic mass values.
- **Group properties:** Elements of group VIII, called rare gases, are characterized by a complete outer layer which gives them exceptional chemical stability.

The elements of group IA (table I.2) have only one electron in their outer layers: they tend to get rid of it to have a saturated outer layer and give positive ions or cations.

This trend also extends to all the elements on the left side of the table, called metals, which are all electron donors. Group VII A elements have seven electrons in their outer

shells: they tend to complete it by capturing an available electron in their neighborhood to give negative ions or anions.

This trend also extends to certain elements on the right side of the table, called non-metals, they all electron acceptors. Certain elements located at the boundary between these two zones have mixed characteristics, varying depending on the electric field to which they are subjected (they are semiconductors). Figure I.3 illustrates these differences in behavior by the band structures of these various types of atoms.

Table I.2: Periodic classification of chemical elements principle [9].

	Group I	**Group II**	**Group III**	**Group IV**	**Group V**	**Group VI**	**Group VII**	**Group VIII**
1st period (k band)	Z=1 A=1 Hydrogen **H**							Z=1 A=4 Helium **He**
2nd period (s, k, and l)	Z=3 A=7 Lithium **Li**	Z=4 A=9 Beryllium **Be**	Z=5 A=11 Boron **B**	Z=6 A=12 Carbon **C**	Z=7 A=14 Nitrogen **N**	Z=8 A=16 Oxygen **O**	Z=9 A=19 Fluor **F**	Z=10 A=20 Neon **Ne**
3rd period (band s, k, l, and m)	Z=11 A=23 Sodium **Na**	Z=12 A=24 Magnesium **Mg**	Z=13 A=27 Aluminum **Al**	Z=14 A=28 Silicium **Si**	Z=15 A=31 Phosphorous **P**	Z=16 A=32 Sulfur **S**	Z=17 A=35 Chlorine **Cl**	Z=18 A=40 Argon **Ar**

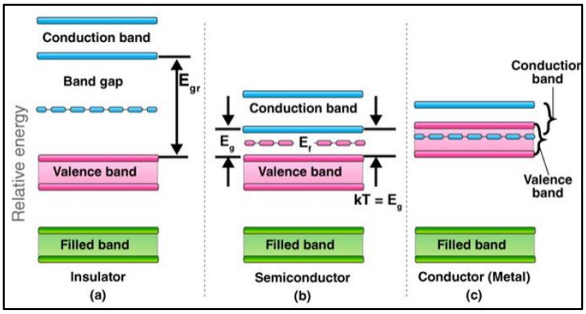
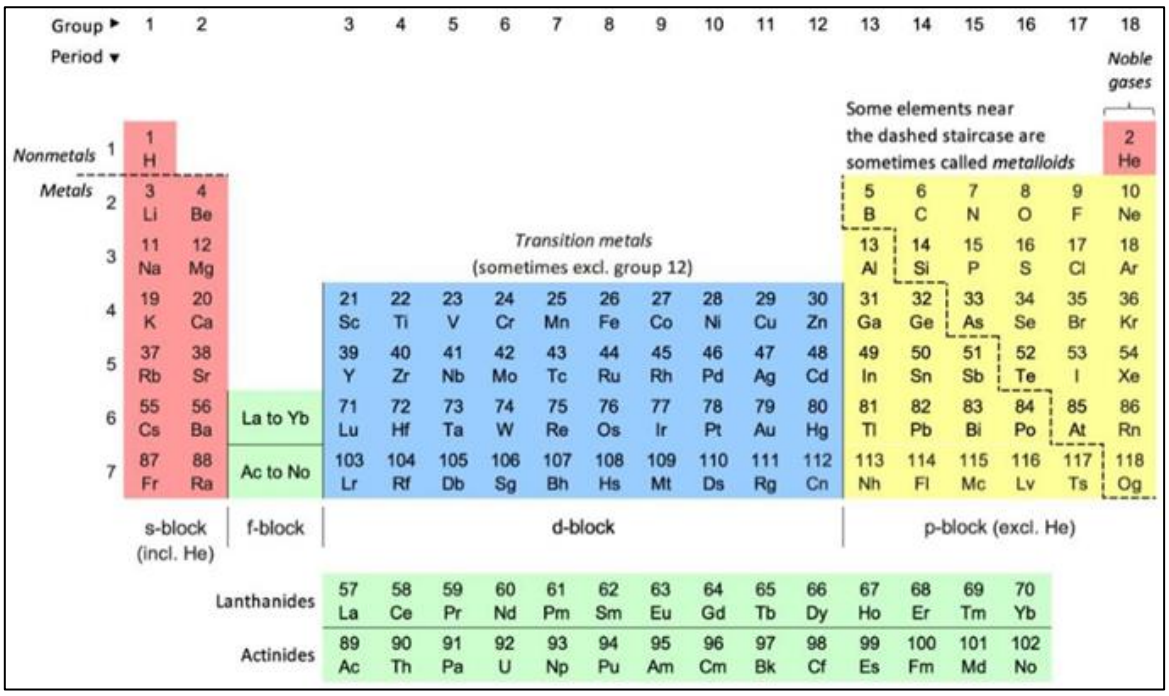


Figure I.3: Diagrams of band structures [9].

- Non-metal atoms (insulator), the band gap has a large ΔE width.
- Semiconductor atoms, the band gap has a small ΔE width.
- Metal atoms, the conduction band has available states.

Table I.3: Periodic classification of elements [9].



I.3.2. Classification of materials and properties

I.3.2.1. Main classes of materials

Many physicochemical properties and usage properties of materials are closely linked to the nature of the chemical bonds between the atoms that constitute them. on this basis that the distinction between the main classes of materials is established.

- **Metal materials:** These are pure metals and their mixtures, or alloys, essentially comprising metallic bonds [10].
- **Organic materials:** These are materials of biological origin, synthetic polymers and elastomers, comprising covalent bonds and weak bonds [11].
- **Mineral materials:** These are rocks, oxides, mineral glasses, ceramics containing ionic bonds and/or covalent bonds [12].
- **Composite materials:** They combine different materials in a structured, fine-scale manner, belonging to different classes among the three previous ones [13].

I.3.2.2. Usage properties

The physicochemical properties and usage properties of materials are multiple and can be subject to various classifications. Some are mainly conditioned by the nature of the atoms and chemical bonds present mainly in the material: density, mechanical and thermal stability, melting temperature, elastic flexibility or rigidity, fragility or ductility, electrical and thermal conductivity, magnetic properties, etc.

Some are sensitive to the structure according to which the atoms are arranged and organized: plastic rigidity, hardness, ductility, tenacity, etc.

I.3.2.3. Principle properties of main materials classes

a. Metal materials

Metallic materials are considered have different property values according to the property itself. This is well established in figure I.4.

b. Organic materials

Relation between property value and property for organic material is represented in figure I.5.

c. Mineral materials

For mineral materials, figure I.6 illustrates the property value-property relationship.

d. Composite materials

Depending on their structure and the nature of their components, the properties of composite materials are extremely variable: for the most part, they are intermediate between the properties of the materials that constitute them. Sometimes, however, certain emergent properties (properties resulting from the entire structure and constituents of the material) can take on unexpected values [13].

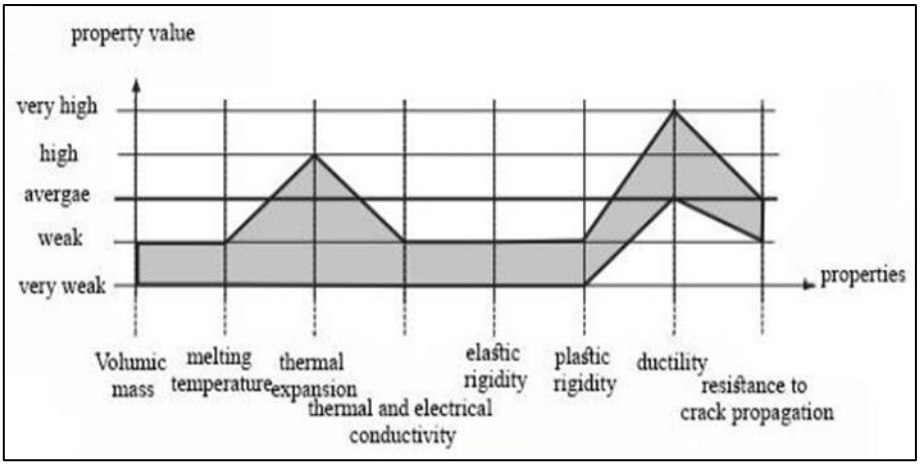


Figure I.4: Property value of metal materials [10].

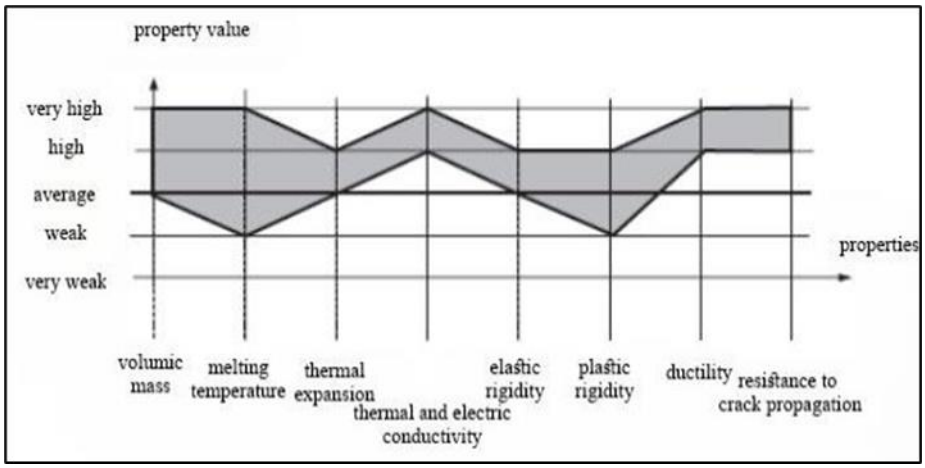


Figure I.5: Property value of organic materials [11].

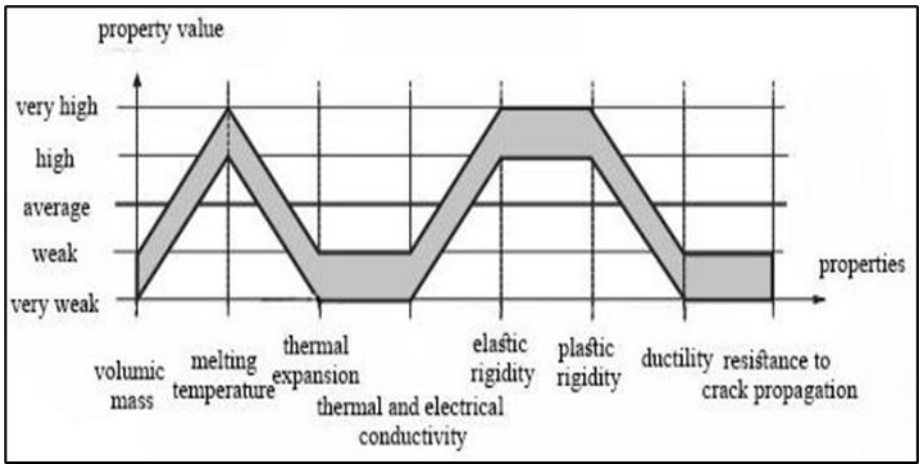


Figure I.6: Property value of mineral materials [12].

I.4. Crystalline solids

A crystal is a set of atoms (or molecules) arranged periodically in three directions and exhibiting both short-range and long-range order. It can be defined from two data: crystal structure and the atomic pattern.

I.4.1. Crystal structure

It is a three-dimensional set of imaginary points, the nodes, arranged periodically in the three directions of space. It can be generated by repetition, an integer number of times, of three basis vectors which define an elementary cell of the arbitrary original network. Therefore, the nodes of the network are all the points of the integer coordinate space in the chosen basis (figure I.4). The nodes are arranged in rows and reticular planes.

There are seven main primitive crystal structures and fourteen lattices named Bravais systems. In table I.4 is regrouped their corresponding characteristics.

An infinite number of possibilities exist for the choice of the elementary cell and its three basic vectors (lengths a, b, c, angles α, β, γ). For the sake of simplicity, the choice generally falls on the mesh presenting the maximum number of symmetry elements (planes and axes of symmetry), which sometimes leads to choosing a multiple mesh (mesh containing several nodes of the network).

Topological considerations relating to the tiling of three-dimensional space by periodic repetition of identical volumes without void or overlap, lead to the conclusion that there can only exist seven different types of meshes, defining the seven primitive crystal systems (figure I.7).

In some of these primitive meshes, additional nodes can be added to the center of the mesh, to the centers of two bases or to the centers of the six faces without losing the properties of periodicity and symmetry of the corresponding networks. We obtain fourteen Bravais networks [14].

Table I.4: Definition of the crystallographic reference frame and characteristics of the meshes of the seven primitive crystal systems and the fourteen Bravais lattices [14].

Primitive crystal system	Bravais networks	Vector lengths	Vector angles	Example
Triclinic	Simple	$a \neq b \neq c$	$\alpha \neq \beta \neq \gamma \neq \pi/2$	
Monoclinic	Simple, with centered bases	$a \neq b \neq c$	$\alpha = \beta = \pi/2 \neq \gamma$	
Orthorhombic	Simple Centered, with centered bases, with centered faces	$a \neq b \neq c$	$\alpha = \beta = \gamma = \pi/2$	UO_2, Fe_3C
Quadratic (Tetragonal)	Simple Centered	$a = b \neq c$	$\alpha = \beta = \gamma = \frac{\pi}{2}$	Martensite
Hexagonal	Simple	$a = b \neq c$	$\alpha = \beta = \frac{\pi}{2}$, $\gamma = \frac{2\pi}{3}$	Zn, Mg
Rhombohedral	Simple	$a = b = c$	$\alpha = \beta = \gamma \neq \frac{\pi}{2}$	As, Sb, Bi
Cubic	Simple Centered Face-centered	$a = b = c$	$\alpha = \beta = \gamma = \frac{\pi}{2}$	Fe, Cu, Al

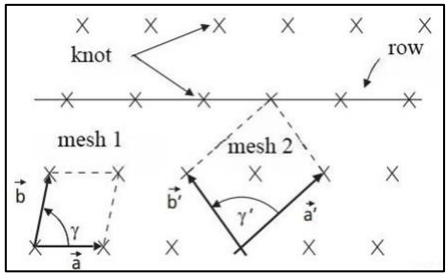


Figure I.7: Diagram of a two-dimensional network [14]:
Mesh No. 1 is an example of an elementary mesh (one knot per mesh).
Mesh N° 2 is an example of a multiple mesh.

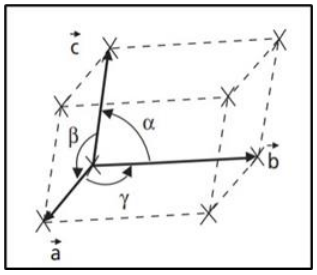


Figure I.8: Mesh construction [14].

I.5. Conductivity

Solid materials are classified according to their conductivities into three types: conductive materials, insulating materials and semiconductor materials.

We have adapted this classification on the basis of a band structure of the material and on a band gap (energy interval) GAP which separates between the valence band and the conduction band [15].

In an insulator, the value of the gap is so large that the electrons cannot pass from the valence band to the conduction band: the electrons do not circulate in the solid. In semiconductors this value is smaller and zero in the conductor. The valence band is rich in electrons but does not participate in conduction phenomena (for electrons). The conduction band, for its part, is empty of electrons. However (metals), the conduction band and the valence band overlap. The electrons can therefore pass directly from the valence band to the conduction band and circulate throughout the solid.

In a semiconductor, as in an insulator, these two bands are separated by a band gap, commonly called by (GAP).

The only difference between a semiconductor and an insulator is the width of this band gap, a width which gives each its respective properties.

The following figure represents E_{GAP} in the three material classes.

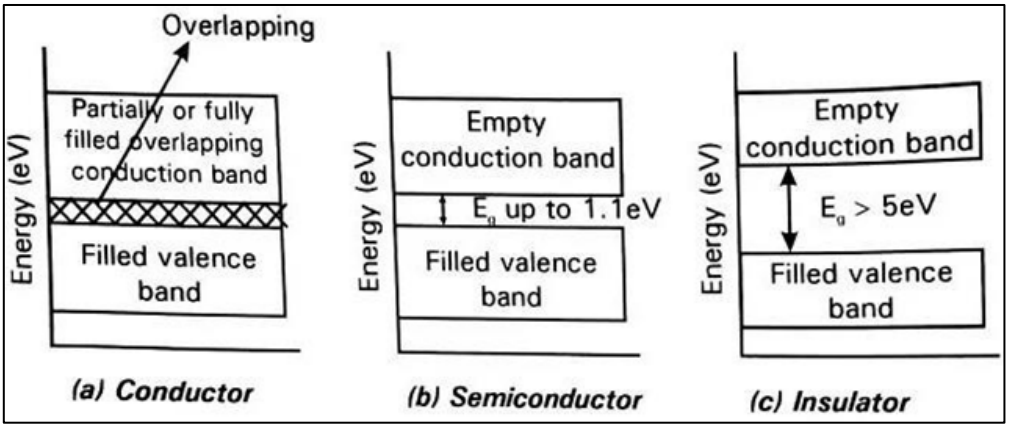


Figure I.9: Theoretical diagram established according to the theory of energy bands indicating, depending on the case, the respective position of the valence band and the conduction band [15].

I.5.1. Semiconductors

A semiconductor, like silicon, is a material that is neither quite a conductor of electricity nor quite an insulator. It can be either one or the other depending on various conditions. The conductive or insulating nature takes its source from the structure of atoms: each element of the periodic table has a certain number of electrons which are arranged around a nucleus. It is this arrangement in the form of layers of electrons, different depending on the elements, which is responsible for electrical conductivity.

The electrons of an atom can have several roles within an atom structure:

- **Core electrons:** These are close to the nucleus and do not really interact with other atoms.
- **Valence electrons:** These are on the outer layers of the atom and make it possible to create interatomic bonds and form molecules.
- **Conduction electrons:** these are responsible for the circulation of electric current.

We see that, in a metal, some electrons are in both the valence band and the conduction band. This means that a metal can conduct current without any other form of physico-chemical treatment. In an insulator, on the other hand, the two bands are separated by a space called the "gap band": this means that electrons cannot be found there. In the case of insulators, the external electrons are all in the valence band and none are in the conduction band: these materials cannot conduct electricity. In the case of semiconductors, in the middle, there is also a band gap, but it is very thin. All it takes is a little something for the valence electrons to pass into the conduction band and this make the semiconductor conductive. We manage to do this by giving energy to the electrons, by exciting them [16].

I.5.2. Direct gap, indirect gap

I.5.2.1. Direct bandgap

In direct bandgap semiconductor, the bottom of the conduction band and top of the valence band lies at the same value of K. In this, electron can directly excite or de-excite by the absorption or emission of photon and there is no phonon involvement in the process

of excitation and de-excitation.

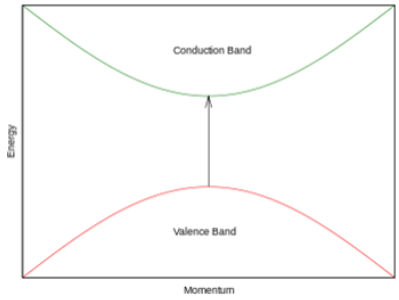


Figure I.10: Direct bandgap [17].

I.5.2.2. Indirect bandgap

in Indirect bandgap semiconductor, top of the valence band and bottom of the conduction band lies at different values of K. If an electron goes from the top of the valence band to the bottom of the conduction band, it has to change its energy as well as wave-vector K [17].

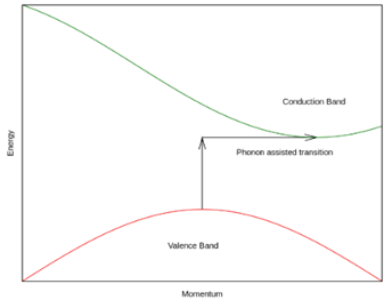


Figure I.11: Indirect bandgap [17].

I.5.3. Chemical bonds

There are different chemical bonds depending on the electronic cloud form and their energy levels. In solids there are two types of bond: Strong bonds and weak bonds

I.5.3.1. Strong bonds

- **Covalent bond:** The sharing of two electrons to complete the outer shell of each atom ensures it. It appears between two non-metal atoms (bond provided by electrons from the valence band).
- **Ionic bond:** The transfer of an electron from one atom to another ensures it. It

appears between an atom of a metal and an atom of a non-metal. After bonding, the two atoms become electrically charged ions.

- **Metallic bond:** The sharing of electrons from the peripheral layer ensures it; the "gas" constituted by these free and delocalized electrons ensures the cohesion of all the remaining cations. It appears between the elements of a cluster of metal atoms (bond provided by the electrons of the conduction band). The electrons in the metallic bond are mobile and available to ensure the possible circulation of an electric current.

I.5.3.2. Weak bonds

These are simple electrostatic attractions between electric charges of opposite signs. They appear between the + and – poles of molecules with inhomogeneous or polarizable charge distributions. They act at a longer distance, but with a lower intensity than strong bonds.

I.6. Density functional theory DFT

Density Functional Theory or DFT forms today one of the most used methods in quantum calculations of the electronic structure of matter (atoms, molecules, solids) both in physics of condensed matter than in quantum chemistry. DFT finds its origins in the model developed by Llewellyn Thomas and Enrico Fermi at the end of the 1920's. However, it was not until the mid-1960s and the contributions of Pierre Hohenberg, Walter Kohn and Lu Sham that the theoretical formalism was established. on which the current method is based. Methods respecting traditions in theories of the electronic structure of matter, especially the Hartree-Fock theory and methods derived from this formalism, are based on a multielectron wave function. The main goal of density functional theory is to replace the multielectron wave function with electron density as the basic quantity for calculations. While the multielectron wave function depends on 3N variables (where N is the total number of particles in the device), the density is only a function of three variables; it is therefore an easier quantity to treat both mathematically and conceptually. The principle of DFT consists of a reformulation of the N-body quantum problem into a one-body problem (or, strictly speaking, two-body if we consider spin problems) with the electron density as a parameter. The central idea of DFT is that the

unique electron density of the essential state of the device entirely determines the average values of observables such as energy.

DFT theory was originally primarily developed within the framework of non-relativistic quantum theory (time-independent Schrödinger equation) and the Born–Oppenheimer approximation. The theory was then extended to the domain of time-dependent quantum mechanics (we then speak of TD-DFT for Time-Dependent Density Functional Theory) and to the relativistic domain. DFT is also used for the thermodynamic description of classical fluids [18].

I.6.1. Schrödinger equation

The geometric structure, vibration modes as well as other observables describe the electronic structure of the system studied with «N electrons» and «M nuclei». Classical mechanics remains insufficient and we must resort to quantum mechanics, the basis of which is the resolution of the Schrödinger equation. This electronic structure is deduced from the time-independent multi-electron Schrödinger equation:

$$\mathbf{H.E = \Psi.E} \quad \text{..... I.1}$$

With:

H: The Hamiltonian operator.

Ψ: The wave function of the system.

E: Clean energy.

I.6.2. Hohenberg and Kohn theorems

The development of density functional theory began in 1964 and 1965 with the publications of Hohenberg and Kohn (1964). The two theorems are as follows:

- **Theorem 01:** The total energy of the fundamental state E is a unique functional of the particle density $\rho(\vec{r})$ for an external potential $V_{ext}(\vec{r})$ given. This theorem means that it is enough to know only the electron density to determine all the wave functions. Consequently, the total energy E of a system of interacting electrons in an external potential is represented as a functional of the electron density of the fundamental state, ρ_0 [19].

- **Theorem 02:** The total energy functional of any multi-particle system has a minimum which corresponds to the fundamental state. The particle density of the fundamental state verifies:

$$\mathbf{E[\rho_0] = minE(\rho)} \quad \text{..... I.2}$$

Hohenberg and Kohn showed that the true density of the fundamental state is that which minimizes the energy $[\rho_0]$, and all other properties are also a functional of this density. The energy of the fundamental state of an electronic system in an external potential is determined by the variational method [20].

I.6.3. Kohn Sham theorem

In 1965 Kohn and Sham (KS) proposed a practical method for using density functional theory. These authors considered the equivalence between a system of electrons interacting in an external potential V and a system of electrons without interaction in an effective potential V_{eff} therefore, the functional of energy [21].

I.6.4. Exchange potential and LDA and GGA correlation

In principle DFT gives us a good description of fundamental state properties, these practical applications are based on approximations for the correlation exchange potential which describes the effects of the Pauli principle and the Coulomb potential beyond a pure electrostatic interaction between electrons.

Exact knowledge of the correlation exchanges potential means that we have solved the multi-body problem exactly. Among the most used approximations currently is the local density approximation (LDA) which locally substitutes the energy density XC of exchange correlation of a non-homogeneous system with that of a gas, of electrons of the same density.

I.6.4.1. Local Density Approximation (LDA)

The local density approximation (LDA) consists of treating an inhomogeneous system, as locally homogeneous (uniform gas of interacting electrons where ρ is constant). Consequently, the Energy of exchange and correlation depends only on the electron density at a point r, neglecting any influence of the inhomogeneity of the system (or

considers that the density varies very slowly). It is expressed according to the Energy of exchange and correlation per particle [22].

I.6.4.2. Generalized Gradient Approximation (GGA)

Generalized gradient approximation was introduced to improve the accuracy of LDA results. It consists of writing the exchange and correlation Energy not only as a function of the electron density but also of its gradient to take into account the non-uniform nature of the electron gas. This approximation is divided into (03) approximations:

- WC-GGA.
- PBE-GGA.
- PBE-SOL-GGA.

I.6.4.3. Approximation WC-GGA

The major gap in the two approximations (GGA and LDA) is the estimation of the value of the energy gap, which is essentially due to the correlation term which is considered too simple, and to correct this gap, Engel and Vosko showed that the GGA does not improve on the second order expansion of the generalized gradient due most of the time to the cancellation of local errors hence the correction made to the correlation term, we mix the second order of the generalized gradient with the exact Hartree-Fock correlation term. This new form called: (EVGGA) turns out to be better for the calculation of the gap, but unfortunately it remains poor if we are interested in the calculations of the fundamental Energy according to the structural parameters [23].

I.6.4.4. Approximation PBE-SOL

Popular modern generalized gradient approximations are biased when describing free atom energies. Restoring the first-principles gradient for exchange over a wide range of density gradients eliminates this bias.

Perdew et al introduced a generalized Perdew-Burke-Emzerof gradient approximation that improves the equilibrium properties of densely packed solids and their surfaces.

I.6.4.5. Approximation of TB-mBJ

In this sense, other improvements have been made such as the TB-mBJ approximation

proposed by Tran and Blaha in 2009. The Tran and Blaha functional noted (mBJ) is a modified version of the Becke and Johnson functional. The latter quickly proved its effectiveness compared to the most often used calculation methods such as LDA and GGA [24]. Messrs. Tran and Blaha propose in their article published on June 3, 2009 in physical review letters, a modified version of the Becke and Johnson functional, in the form:

$$v_{x,\sigma}^{(MBJ)}(r) = c\, v_{x,\sigma}^{BR} + (3c-2)\left(\frac{1}{\pi}\right)\sqrt{\frac{5}{12}}\sqrt{\frac{2t_{\sigma(r)}}{\rho_\sigma}} \quad \text{..... I.3}$$

with:

$\rho_\sigma = \sum_{i=1}^{N_\sigma} |\Psi_{i,\sigma}|^2$ Electron density.

$t_\sigma(r) = \frac{1}{2}\sum_{i=1}^{N} |\Psi^*_{i,\sigma}\nabla\Psi_{i,\sigma}|^2$ Kinetic energy density.

$v_{x,\sigma}^{(MBJ)}(r)$ The potential of Becke-Roussel.

I.7. Wien2k calculation code

The WIEN2k package is a computer program written in Fortran which performs quantum mechanical calculations on periodic solids. It uses the full-potential (linearized) augmented plane-wave and local-orbitals [FP-LAPW+lo] basis set to solve the Kohn–Sham equations of density functional theory.

Peter Blaha and Karlheinz Schwarz from the Institute of Materials Chemistry of the Vienna University of Technology originally developed WIEN2k. The first public release of the code was done in 1990 [25].

Then, the next releases were WIEN93, WIEN97, and WIEN2k.The latest version WIEN2k_23.2 was released in February 2023. It has been licensed by more than 3400 user groups and has about 16000 citations on Google scholar (Blaha WIEN2k).



Figure I.12: Wien2k code logo [25].

I.7.1. The main steps to follow in the WIEN2K code

When using this code, we generally go through three steps.

I.7.1.1. Initialization

This step is done for the preparation of the SCF cycle. During this step, a series of subprograms are executed, among which we cite [25]:

- **N**: Is a program that lists the distances between nearest neighbors, which helps determine the value of the atomic radius of the sphere (R_{MT}).
- **SGROUP**: It determines the space group of the structure that is defined in the case (CIF) file.
- **SYMMETRY**: Is a subprogram which lists the symmetry operations of the space group of our structure from the information contained in the case file (CIF).
- **LSTART**: A program that generates atomic densities and determines how different orbitals are treated in calculating band structure, such as core states with or without local orbitals.
- **KGEN**: This subprogram generates a mesh of points K in the irreducible part of the first Brillouin zone (IBZ). We specify the number of points K in the entire first Brillouin zone.
- **DSTART**: This subroutine subprogram produces a first crystal charge density (case.clmsum), an initial density for the SCF (self-consistent field) by superposition of atomic densities.

I.7.1.2. SCF calculation

The initialization part allowed the creation of all the inputs for the SCF cycle, the process is then launched and iterates until the solution converges. This cycle is made up of five sub-programs [25]:

- **LAPW0:** Is a sub-program which calculates the total potential as the sum of the Coulomb potential VC and the exchange and correlation potential V_C^X.
- **LAPW1:** Is a sub-program that finds the Hamiltonian, overlap matrix, eigenvalues and eigenvectors by a diagonalization method.

- **LAPW2**: Is a sub-program that calculates valence electron densities from eigenvectors, it uses **case.energy** et **case.vector** and calculates E_F (Fermi level).
- **LCORE:** Is a sub-program that calculates core states and densities.
- **MIXER:** Is a sub-program that mixes the valence and core densities to produce a new density that will be used in the next iteration.

I.7.1.3. Exploring material properties

After the SCF calculation, we have all the data, in particular the Total Energy at equilibrium and the structural parameters, which allow us to examine the properties of the materials we wish to study.

After having summarized the main steps seen in the progress or execution of the WIEN2K code, we recall in the following part the main files that are necessary to execute certain programs or the files generated as output [25].

I.8. Origin 2019

Origin is a proprietary computer program for interactive scientific graphing and data analysis. It is produced by OriginLab Corporation, and runs on Microsoft Windows. It has inspired several platform-independent open-source clones and alternatives like LabPlot and SciDAVis [26].

Graphing support in Origin includes various 2D/3D plot types.



Figure I.14: Origin ver.19 logo.

Data analyses in Origin include statistics, signal processing, curve fitting and peak analysis. Origin's curve fitting is performed by a nonlinear least squares fitter which is based on the Levenberg-Marquardt algorithm.

Origin imports data files in various formats such as ASCII text, Excel, NI TDM, DIADem, NetCDF, SPC, etc. It also exports the graph to various image file formats such as JPEG, GIF, EPS, TIFF, etc. There is also a built-in query tool for accessing database data via ADO [26].

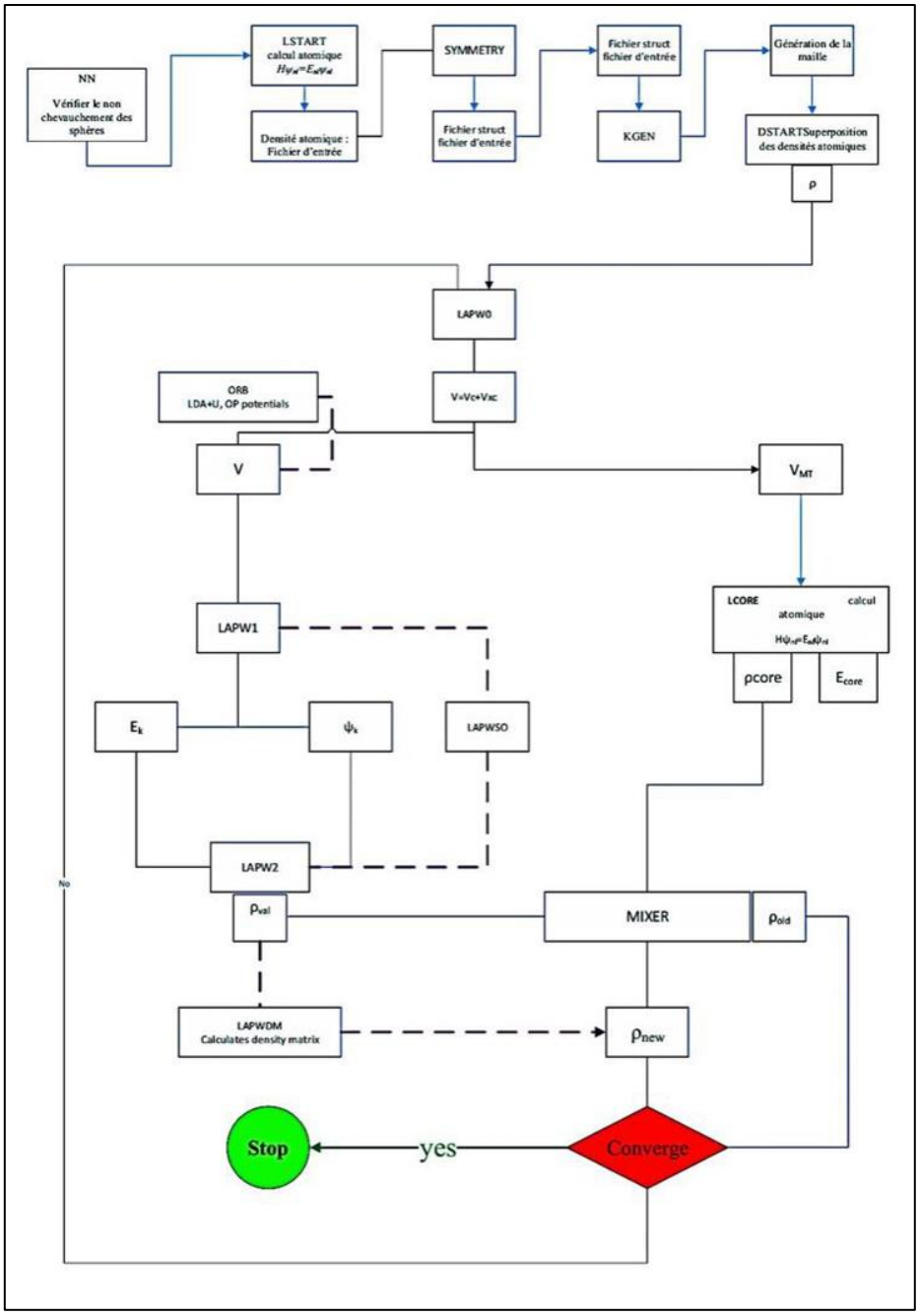


Figure I.13: Wien2k code structure [26].

I.9. Conclusion

In this chapter We have generally studied materials, we can say that density functional theory is a very effective tool for the study of interacting electron systems. Indeed, it reduces the problem with N interacting bodies to that of N independent bodies which move in an effective potential.

References

[1]: Semiconductor Physics and Devices, D.A. Neamen. *Semiconductor Physics and Devices: Basic Principles*. McGraw-Hill.

[2]: Materials Selection in Mechanical Design, M.F. Ashby. *Materials Selection in Mechanical Design*. Butterworth-Heinemann.

[3]: *Chemical physics*. Retrieved from CEA https://www.cea.fr/comprendre/Pages/physique-chimie/essentiel-sur-materiaux.aspx

[4]: W.F. Smith. *Principles of materials science and engineering* (1990).

[5]: Materials Science and Engineering: An Introduction, W.D. Callister Jr., D.G. Rethwisch. *Materials Science and Engineering: An Introduction*. Wiley.

[6]: M.H. Sadd. *Elasticity: theory, applications, and numerics.*

[7]: Retrieved from https://clarolineconnect.univ-lyon1.fr/:https://clarolineconnect.univ-lyon1.fr/clarolinepdfplayerbundle/pdf/3112949

[8]: *Atome*. Retrieved from Wikipedia https://fr.wikipedia.org/wiki/Atome#

[9]: M. Dupeux. *Science et génie des matériaux* (2018).

[10]: *Metal*. Retrieved from wikipedia https://fr.wikipedia.org/wiki/M%C3%A9tal#cite_ref-1

[11]: *Organic matter*. Retrieved from wikipedia https://en.wikipedia.org/wiki/Organic_matter

[12]: *Minéral*. Retrieved from Wikipedia https://fr.wikipedia.org/wiki/Min%C3%A9ral

[13]: *Composite material*. Retrieved from wikipedia https://en.wikipedia.org/wiki/Composite_material

[14]: J. Hook, H. Hall. *Solid State Physics* (2010). [15]: *Band gap*. Retrieved from wikipedia https://en.wikipedia.org/wiki/Band_gap#References

[16]: *Semiconductors*. Retrieved from byjus https://byjus.com/jee/semiconductors/

[17]: *Direct and indirect band gaps*. Retrieved from wikipedia

https://en.wikipedia.org/wiki/Direct_and_indirect_band_gaps

[18]: Density functional theory and application to atoms and molecules. *Physics Reports* (2014) 123-239.

[19]: J. Stephen, C.C. Klippenstein. *Density functional theory*. In A.C. Dimian. *Computer Aided Chemical Engineering* (1997).

[20]: C.C.M. Rindt, S.G.-N. Hohenberg–Kohn theorems. In L.F. Cabeza. *Advances in Thermal Energy Storage Systems* (2015).

[21]: W.K. Sham. Self-consistent equations including exchange and correlation effects. *Physical Review* A1133 to A1138.

[22]: *Local-density approximation*. Retrieved from Wikipedia https://en.wikipedia.org/wiki/Local-density_approximation

[23]: V. Valentin, S.B. Karasiev. Advances in quantum chemistry. In *Advances in Quantum Chemistry* (2015) 221-245.

[24]: D. Reyes-coronado, G. Rodríguez-gattorno, M.E. Espinosapesqueira, *et al.* Phase-pure TiO2 nanoparticles: anatase, brookite and rutile. Nanotechnology 19(14) (2008) 145605.

[25]: P. Blaha, K. Schwarz, P. Sorantin, S.B. Trickey. *Comput. Phys. Commun.* 59 (1990) 399.

[26]: **OriginLab.** (2019). *Origin* (Version 2019) [Logiciel]. OriginLab Corporation, Northampton, MA, USA. Disponible sur: https://www.originlab.com

Chapter II:

Results and discussion

II.1. Introduction

The materials considered in this study were investigated with regard to their structural, electronic, and optical properties via ab initio calculations using the calculation code Abinit [1].

The materials studied are the monoclinic [2], rhombohedral [3], and cubic [4] cesium iodates noted; M-$CsIO_3$, R-$CsIO_3$, and C-$CsIO_3$ respectively.

II.2. Calculation details and parameters

II.2.1. Methods adopted

The calculation launch for each material with Abinit is started by the manual introduction of an input density generated by the following data:

- Atomic number Z of each element in the material considered.
- Crystal system (Bravais lattice and space group).
- Cell parameters (a, b, c, α β and γ).
- Positions of atoms (x, y, and z).

II.2.1.1. Code Abinit

Calculations made with Abinit have the following details:

- **Method:** Pseudo-potentials; PP-PW (PseudoPotential-Plane Waves).
- **Approximation:** LDA (Local Density Approximation).
- **Exchange-correlation potential:** PW-LDA [5].
- **Calculated properties:** Structural parameters, elastic constants $\mathbf{C_{ij}}$, piezoelectric coefficients $\boldsymbol{d_{ij}}$, optoelectric coefficients $\mathbf{r_{ij}}$, and non linear optical coefficients $\mathbf{d_{ij}}$.

- **Pseudopotentials:** *normconserving* Troullier-Martin [6] generated with the code FHI (Fritz–Haber-Institute code) [7] with valence electrons of atoms Cs, I, and O (table II.1).
- **Theory:** DFPT (Density Functional Perturbation Theory) [8].

II.2.2. Convergence step

Before any calculation of properties, convergence studies followed by optimization must be carried out. In the convergence stage, the most important criteria are the relative variations of the total energy as a function of the calculation parameters: E_{cutoff} and ngkpt parameters. The values adopted for the calculation parameters are cross-referenced in (table II.2).

Table II.1: Valence state of $CsIO_3$ constituent elements.

Element	Valence state
Cs	$4d^{10}5s^25p^66s^1$
I	$4d^{10}5s^25p^5$
O	$2s^22p^4$

Table II.2: The **k-points** grid (points of sampling of Irreducible Brillouin Zone IBZ).

Compound	Grid (ngkpt)	E_{cutoff} (Ha)
M-$CsIO_3$	6x8x6	50
R-$CsIO_3$	8x8x8	50
C-$CsIO_3$	8x8x8	50

II.2.3. Optimization step

The optimization step serves to relax the structure. An optimized structure corresponds to a minimum total energy, with relaxed atoms in a balanced environment resulting in minimal net forces and zero Hellmann-Feynman forces (exerted on the atoms).

Optimization is performed using the BFGS program [9]. Often, several cycles are necessary to obtain a well-optimized structure.

It should be noted that optimization with ABINIT serves to extract an optimal structure.

II.3. Structural study of the $CsIO_3$ polymorphs

The iodates of Cs are not isostructural. A comparative study of their properties was therefore undertaken. In this part of the calculations, we will examine the effect of changing the symmetry and structure without changing the formula.

We thoroughly investigated the compounds M-$CsIO_3$, R-$CsIO_3$, and C-$CsIO_3$ by calculating their properties using the ABINIT code.

In each step of the calculations (detailed below), our results were compared on the one hand with experimental results, and on the other hand with theoretical results (if they exist).

II.3.1. Historical

The three compounds considered in this section on property calculations are polymorphs. The first iodate; M-$CsIO_3$(figure II.1); crystallizes in the *P1m1* space group (N°. 6) of the *m* (monoclinic) class [2]. The second phase; R-$CsIO_3$ (figure II.2); in the R3m space group (N°. 160) of the 3m (trigonal) rhombohedral class [3]. The last polymorph; C-$CsIO_3$ (figure II.3); is cubic (Pm-3m N°. 221) [4].

They have all a typical structure for metallic iodates with an asymmetric environment on the iodine atom. The latter has six I-O bonds: three short (strong with average lengths of 1.9Å) and three long (weak with 2.9Å in length), generated by the electron pair activity on the iodine atom [10] (figure II.4) [11].

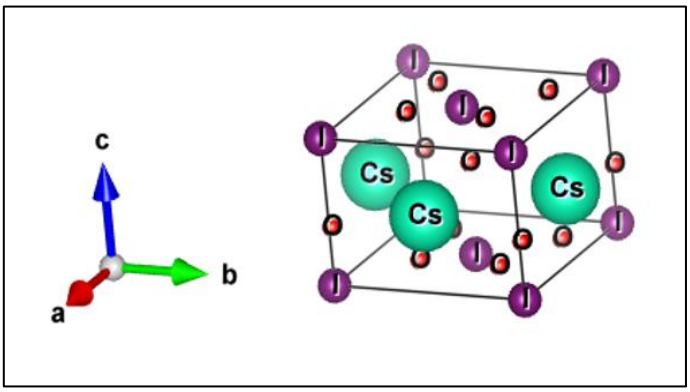


Figure II.1 Monoclinic primitive cell of M-$CsIO_3$.
Drawn from CIF file by VESTA software [12].

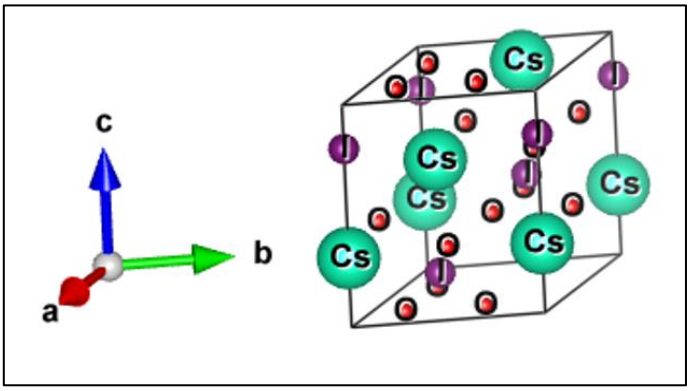


Figure II.2 Rhombohedral primitive cell of C-$CsIO_3$.
Drawn from CIF file by VESTA software [12].

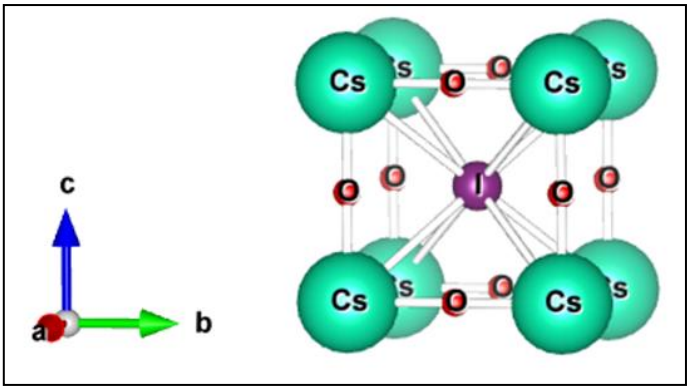


Figure II.3 Cubic primitive cell of C-$CsIO_3$.
Drawn from CIF file by VESTA software [12].

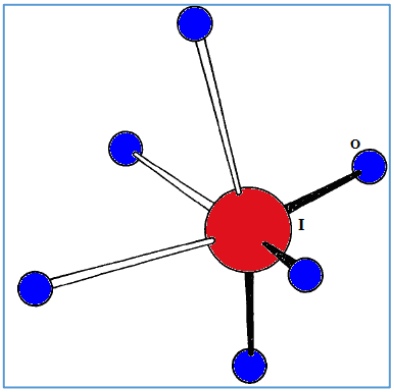


Figure II.4: Environnement of the iodine atom in iodate compounds [11].

The first studies on cesium iodates date back to the work of Wheeler and Vipond [13,14]. Studies of optical properties and crystallization are also cited [15,16]. This iodate has not received as much attention as its Rb and K analogs. Mixed iodate compounds based on Cs have been reported [17]. However, other ONL (non-iodate) compounds based on Cs have also been developed [18].

Table II.3 below lists the Cs iodates cited in the literature.

Tableau II.3: Structural properties of cesium iodates described in the literature.

N°	a (A°)	b (Å)	c (Å)	α/β/γ(°)	V(Å^3)/Z	Space group/N°	Class	Réf
1	6.613	6.613	4.676	90/90.8/90	204.47/2	*P1m1*/6	Mono	[2]
2	6.6051	6.6051	8.087	90/90/120	305.53/3	*R3mH*/160	Rhombo	[3]
3	4.662	4.662	4.662	90/90/90	101.33/1	*Pm-3m*/221	Cubique	[4]

In the present study, we considered the three polymorphs.

II.3.2. Structural properties of cesium iodates

The lattice parameters a, b, and c, and also the atomic positions are calculated, and the results are summarized in tables II.4 and II.5 respectively.

Table II.4: Simulated and experimental structural parameters of cesium iodates.

Crystal system	Parameter	Exp.	This work	Deviation (%)
Monoclinic [2]	a=b (Å)	6.613	6.1273	-7.34
	c (Å)	4.476	4.3244	-7.52
	V(Å^3)	264.47	162.34	-38.62
Rhombohedral [3]	a=b (Å)	6.6051	6.041	-8.54
	c (Å)	8.087	7.68	-5.03
	V(Å^3)	305.54	294.79	-20.56
Cubic [4]	a=b=c (Å)	4.662	5.5724	+19.53
	V(Å^3)	101.33	173.03	+70.76

Table II.5: Atomic coordinates for cesium iodates.

Crystal System	Atom	x;y;z		Deviation (%)
		Experimental	Calculated	
Monoclinic	Cs 1	0.485;0;0.485		
	Cs 1	-0.015;0.5;0.515		
	I 1	0;0;0	/	/
	I 2	0.5;0.5;0	/	/
	O 1	-0.024;0;0.386		
	O 2	0.176;0.209;-0.034		
	O 3	0.676;0.709;0.034		
	O 4	0.476;0.5;0.14		
Rhombohedral	Cs	0;1;0.3119	0.3148	+0.23
	O	0.1377:0.8623;0.674		
	I	0;1;0.8033	0.7957	-0.95
Cubic	Cs	0;0;0	/	/
	O	0.5;0.5;0.5	/	/
	I	0;0;0.5	/	/

From these results, we report tolerable deviations for lattice parameters ranging between 5.03% and 19.53% for mesh parameters, thus generating optimized volumes with deviations ranging from 20.56% to 70.76%.

At this stage, we deem it necessary to discuss the I-O bond lengths by comparing the experimental values with those obtained with the optimized structures. Indeed, we report the following figures:

- For M-$CsIO_3$: 1.78721 Å calculated versus 1.891 Å [2]: deviation of -5.49%.
- For R-$CsIO_3$: 1.83972 Å calculated versus 1.891 Å [3]: deviation of -2.69%.
- For C-$CsIO_3$: 1.3954 Å calculated versus 1.891 Å [4]: deviation of -26.21%.

II.4. Elastic properties

II.4.1. Elastic constants

The elastic constants $\boldsymbol{C_{ij}}$ determine the response of a crystal to external forces, characterized by the compressive, shear, and Young's moduli, and by the Poisson's ratio. These parameters obviously play an important role in determining the hardness of materials. These parameters also provide us with the following information:

- The bonding characteristics between adjacent atomic planes.
- The mechanical stability of the structure.
- The anisotropy in the material.

Monoclinic cesium iodate (crystallizing in class **m**) has 13 independent elastic constants $\boldsymbol{C_{ij}}$. The distribution of these coefficients in their respective tensors is as follows [19,20]:

$$\begin{bmatrix} C_{11} & C_{12} & C_{13} & 0 & C_{15} & 0 \\ & C_{22} & C_{23} & 0 & C_{25} & 0 \\ & & C_{33} & 0 & C_{35} & 0 \\ & & & C_{44} & 0 & C_{46} \\ & & & & C_{55} & 0 \\ & & & & & C_{66} \end{bmatrix} \quad \text{II.1}$$

The conditions for mechanical stability are as follows [20,21]:

- $C_{11}, C_{22}, C_{33}, C_{44}, C_{55}, C_{66}>0$ II.2
- $[C_{11}+C_{22}+C_{33}+2(C_{12}+C_{13}+C_{23})] > 0$ II.3
- $(C_{33}.C_{55}-C_{35}^2) > 0$ II.4
- $(C_{44}.C_{66}-C_{46}^2) > 0$ II.5
- $(C_{22}+C_{33}-2.C_{23}) > 0$ II.6
- $[C_{22}(C_{33}.C_{55}-C_{35}^2)+2.C_{23}.C_{25}.C_{35}-C_{23}^2.C_{55}-C_{25}^2.C_{33}] > 0$ II.7

- $\{2[C_{15}.C_{25}.(C_{33}.C_{12}-C_{13}.C_{23})+C_{15}.C_{35}(C_{22}.C_{13}-C_{12}.C_{23})+C_{25}.C_{35}(C_{11}.C_{23}-C_{12}.C_{13})]-[C_{15}^2(C_{22}.C_{33}-C_{23}^2)+C_{25}^2(C_{11}.C_{33}-C_{13}^2)+C_{35}^2(C_{11}.C_{22}-C_{12}^2)]+C_{55}.\mathbf{g}\}>0$ II.8

with: $\mathbf{g}=C_{11}.C_{22}.C_{33}-C_{11}.C_{23}^2-C_{22}.C_{13}^2-C_{33}.C_{12}^2+2.C_{12}.C_{13}.C_{23}$ II.9

The eight stability conditions (II.2 to II.9) are well satisfied. Our material is therefore mechanically stable.

R-$CsIO_3$ crystallizes in the 3m class and possess six independent elastic constants $\boldsymbol{C_{ij}}$ (II.10). The distribution of these coefficients in their respective tensors is as follows [19,22]:

$$\begin{bmatrix} C_{11} & C_{12} & C_{13} & C_{14} & 0 & 0 \\ & C_{11} & C_{13} & -C_{14} & 0 & 0 \\ & & C_{33} & C_{14} & 0 & 0 \\ & & & C_{44} & 0 & 0 \\ & & & & C_{44} & C_{14} \\ & & & & & C_{66}=\tfrac{1}{2}(C_{11}-C_{12}) \end{bmatrix} \quad \text{II.10}$$

The mechanical stability criteria are [20]:

- $C_{11}>|C_{12}|$ II.11
- $C_{13}^2<\frac{1}{2}C_{33}(C_{11}+C_{12})$ II.12
- $C_{14}^2<\frac{1}{2}C_{44}(C_{11}-C_{12})=C_{44}C_{66}$ II.13
- $C_{44}>0$ II.14

The four stability conditions (II.11 to II.14) are well satisfied. Our material is therefore mechanically stable.

Cubic cesium iodate (crystallizing in the class $m\bar{3}m$) has 04 independent elastic constants ***Cij***. The distribution of these coefficients in their respective tensors is as follows [19,20]:

$$\begin{bmatrix} C_{11} & C_{12} & C_{13} & 0 & 0 & 0 \\ & C_{11} & C_{12} & 0 & 0 & 0 \\ & & C_{11} & 0 & 0 & 0 \\ & & & C_{44} & 0 & 0 \\ & & & & C_{44} & 0 \\ & & & & & C_{44} \end{bmatrix} \quad \text{II.15}$$

The conditions for mechanical stability are as follows [20]:

- $C_{11}>0$, $C_{44}>0$ II.16
- $C_{11}>|C_{12}|$ II.17
- $C_{11}+2.C_{12}>0$ II.18

The mechanical stability conditions for phases M and R are well satisfied. For phase C, the second condition is not satisfied because $C_{11}=C_{12}$. Our materials M and R are therefore mechanically stable while C is unstable.

The values of the elastic coefficients obtained are summarized in table II.6.

Tableau II.6: Elastic constants C_{ij} calculated for the M, R, and C phases of the compound $CsIO_3$ in GPa.

Constante élastique C_{ij}	$CsIO_3$		
	M	**R**	**C**
C_{11}	75.82	114.18	208.57
C_{12}	30.11	37.16	-30.06
C_{13}	33.22	34.70	-30.06
C_{14}	0	-0.00001	0
C_{15}	0.318	0	0
C_{22}	76.10	0	208.57
C_{23}	50.45	0	-30.06
C_{25}	0.091	0	0
C_{33}	110.23	97.40	208.57
C_{35}	-0.145	0	0
C_{44}	52.91	35.71	80.80
C_{46}	-0.031	0	0
C_{55}	34.97	0	80.80
C_{66}	31.36	38.51	80.80

There are no experimental or theoretical values for the elastic constants of these materials in the literature.

A superficial analysis of the results obtained reveals that the values differ from one phase to another.

We also observe that $\mathbf{C_{11}}$ and $\mathbf{C_{33}}$ (and $\mathbf{C_{22}}$ for phase M) are larger than $\mathbf{C_{44}}$ and $\mathbf{C_{66}}$ (and $\mathbf{C_{55}}$ for phase M), which means that our phases resist compression better than shear.

Furthermore, phase M is more compressible along the *zz* axis than along the other two axes, which have similar elasticities (inversely consistent with the lattice parameters a ≈ b > c).

Phase C exhibits isotropic compression (a = b = c and $\mathbf{C_{11}} = \mathbf{C_{22}} = \mathbf{C_{33}}$).

Phase R compresses better in the ***xx*** axis than in the *zz* axis (a < c). In general, phase C is characterized by higher elastic coefficients than phases M and R, but its mechanical instability.

In conclusion, we can say that symmetry directly affects the elasticity of materials. Its effects are directly related to the lattice parameters.

From the preliminary analysis of the results obtained, we observe that the values are similar from one material to another, but we also note that some coefficients are higher for one material than for others, and vice versa.

In order to better compare the elastic constants, we plotted their values for each iodate compound. Figure II.5 illustrates this comparison.

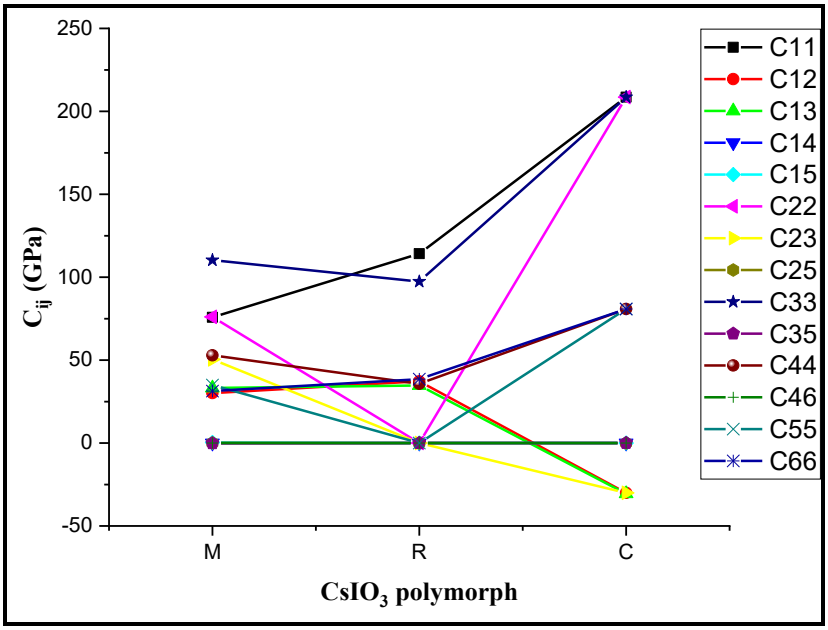


Figure II.5: Elastic constants variation $\boldsymbol{C_{ij}}$ for the M, R, and C polymorphs of $CsIO_3$.

We observe from this projection that the compression coefficients $\mathbf{C_{11}}$ and $\mathbf{C_{33}}$ are significantly higher than the shear coefficients $\mathbf{C_{44}}$ and $\mathbf{C_{66}}$, and this is true for all iodates. This means that our materials resist compression better than shear. Furthermore, the $\mathbf{C_{11}}$ coefficients are higher than the $\mathbf{C_{33}}$ coefficients, which means that the compression of our materials along the **a** (**b**) axis is greater than their compression along the **c** axis. The compression of our materials is therefore expected to be anisotropic.

II.4.1. Other mechanical properties

Other mechanical properties are also calculated using the three approximations of Voigt [23], Reuss [24], and Hill [25], namely:

- The bulk modulus (**B**), which measures a substance's resistance to uniform compression.
- The shear modulus (**G**), which interprets the resistance to plastic deformation following a force applied parallel to a given surface of the material.
- Young's modulus (**E**), which describes the stiffness of the material.
- The following properties are derived from these three moduli:
- Poisson's ratio (σ), which provides information on the bonding forces present in solid materials.
- The ***B/G*** ratio, used to evaluate the ductility or brittleness of the compound.

The compression or elasticity coefficient **B**, shear coefficient **G**, Young's coefficient **E**, and Poisson's ratio σ, as well as the **B/G** ratio, were calculated for a more in-depth analysis of the mechanical properties of the $CsIO_3$ phases.

The equations used to calculate these properties are as follows [21]:

a. For the monoclinic phase class m:

- $\boldsymbol{B_V}=1/9\ [C_{11}+C_{22}+C_{33}+2.(C_{12}+C_{13}+C_{23})]$ II.19
- $\boldsymbol{G_V}=1/15[C_{11}+C_{22}+C_{33}+3.(C_{44}+C_{55}+C_{66})-(C_{12}+C_{13}+C_{23})]$ II.20
- $\boldsymbol{B_R}=\mathbf{\Omega}.[\mathbf{a}.(C_{11}+C_{22}-2.C_{12})+\mathbf{b}.(2.C_{12}-2.C_{11}-C_{23})+\mathbf{c}.(C_{15}-2.C_{25})+\mathbf{d}.(2.C_{12}+2.C_{23}-C_{13}-2.C_{22}+2.\mathbf{e}.(C_{25}-C_{15})+\mathbf{f}]^{-1}$ II.21

- $\boldsymbol{G_R}=15.\{4.[\mathbf{a}.(C_{11}+C_{22}+C_{33})+\mathbf{b}.(C_{11}-C_{12}-C_{23})+\mathbf{c}.(C_{15}+C_{25})+\mathbf{d}.(C_{22}-C_{12}-C_{23}-C_{13})+2.(C_{15}-C_{25})+\mathbf{f}]/\Omega+3.\{[\mathbf{g}/\boldsymbol{\Omega}+[(C_{44}+C_{66})/(C_{44}.C_{66}-C_{46}^2)]\}\}^{-1}$ II.22

with:

- $\mathbf{a}=C_{33}.C_{55}-C_{35}^2$ II.23
- $\mathbf{b}=C_{23}.C_{55}-C_{25}.C_{35}$ II.24
- $\mathbf{c}=C_{13}.C_{35}-C_{15}.C_{33}$ II.25
- $\mathbf{d}=C_{13}.C_{55}-C_{15}.C_{35}$ II.26
- $\mathbf{e}=C_{13}.C_{25}-C_{15}.C_{23}$ II.27
- $\mathbf{f}=C_{11}.(C_{22}.C_{55}-C_{25}^2)-C_{12}.(C_{12}.C_{55}-C_{15}.C_{25})+C_{15}.(C_{12}.C_{25}-C_{15}.C_{22})+C_{25}.(C_{23}.C_{35}-C_{25}.C_{33})$ II.28
- $\boldsymbol{\Omega}=2.[C_{15}.C_{25}.(C_{33}.C_{12}-C_{13}.C_{23})+C_{15}.C_{35}.(C_{22}.C_{13}-C_{12}.C_{23})+C_{25}.C_{35}.(C_{11}.C_{23}-C_{12}.C_{13})]-[C_{15}^2.(C_{22}.C_{33}-C_{23}^2)+C_{25}^2.(C_{11}.C_{33}-C_{13}^2)+C_{35}^2.(C_{11}.C_{22}-C_{12}^2)]+\mathbf{g}.C_{55}$ II.29
- $\mathbf{g}=C_{11}.C_{22}.C_{33}-C_{11}.C_{23}^2-C_{22}.C_{13}^2-C_{33}.C_{12}^2+2.C_{12}.C_{13}.C_{23}$ II.30

b. For the rhombohedral phase

For class 3m, the equations below (II.31 to II.40) allow the calculation of all these mechanical properties.

$\boldsymbol{B_V} = 1/9\ [2(C_{11}+C_{12}) + 4.C_{13} + C_{33}]$ II.31

$\boldsymbol{B_R} = \mathbf{C^2/M}$ II.32

$\mathbf{C^2} = (C_{11}+C_{12}).C_{33} - 2.C_{13}^2$ II.33

$\mathbf{M} = C_{11}+C_{12}+2.C_{33}-4.C_{13}$ II.34

$\boldsymbol{B_H} = ½\ (\boldsymbol{B_V}+\boldsymbol{B_R})$ II.35

$\boldsymbol{G_V} = 1/30\ [\mathbf{M} + 12(C_{44}+C_{66})]$ II.36

$\boldsymbol{G_R} = 5/2\{[\mathbf{c^2}.(C_{44}.C_{66}-C_{14}^2)]/[3.\boldsymbol{B_V}.(C_{44}.C_{66}-C_{14}^2)+\mathbf{c^2}.(C_{44}.C_{66})]\}$ II.37

$\boldsymbol{G_H} = ½\ (\boldsymbol{G_V}+\boldsymbol{G_R})$ II.38

$E_i = (9.B_i.G_i)/(3.B_i+G_i)$, avec $i = V$, R, ou H II.39

$\sigma = (3.B_H-2.G_H)/[2.(3.B_H+G_H)]$ II.40

c. For the cubic phase:

- $B_V = B_R = (C_{11}+2.C_{12})/3$ II.41
- $G_V = (C_{11}-C_{12}+3.C_{44})/5$ II.42
- $G_R = 5.(C_{11}-C_{12}).C_{44}/[4.C_{44}+3.(C_{11}-C_{12})]$ II.43

The results obtained are grouped in table II.7.

Table II.7: Compression ***B***, shear ***G***, and Young ***E*** moduli, Poisson coefficient σ and ***B/G*** ratio.

$CsIO_3$	***B***			***G***			***E (GPa)***			σ	***B/G***
	B_V	B_R	B_H	G_V	G_R	G_H	E_V	E_R	E_H		
M	54.41	51.38	**52.90**	33.74	30.09	**31.91**	83.88	75.52	**79.71**	**0.2488**	**1.6575**
R	59.88	59.48	**59.68**	36.60	35.50	**36.05**	91.22	88.82	**90.02**	**0.2486**	**1.6555**
C	49.48	49.48	**49.48**	96.21	92.78	**94.49**	175.13	171.29	**173.22**	**-0.083**	**0.5237**

Since the cubic phase is unstable, the values are taken into consideration for comparative purposes.

We observe that:

- For compression moduli ***Bi***, phase R has the highest values, followed by M and then C.
- The values of ***Gi*** and Ei (***i*** = **V**, **R**, or **H**) are all higher and significantly greater with phases C, then R, and then M, which are comparable (figure II.6).
- The parameters σ and **B/G** are almost identical for phases M and R, but they are higher for phase C.

From these observations, we conclude that:

- The ***Bi*** values of the three phases of the $CsIO_3$ compounds are related to the lattice parameters **a** and **c**, and therefore to the optimized volume **V**. Increasing the latter leads to an increase in ***Bi*** values, and vice versa (figure II.7).

- ***Gi*** and ***Ei*** values decrease with decreasing symmetry (C > R > M).
- The values of σ and **B/G** are higher in structures with low symmetry and gradually decrease towards structures with high symmetry for the same atomic structure.
- The near-zero value of σ for the cubic compound indicates that our compound is metallic.

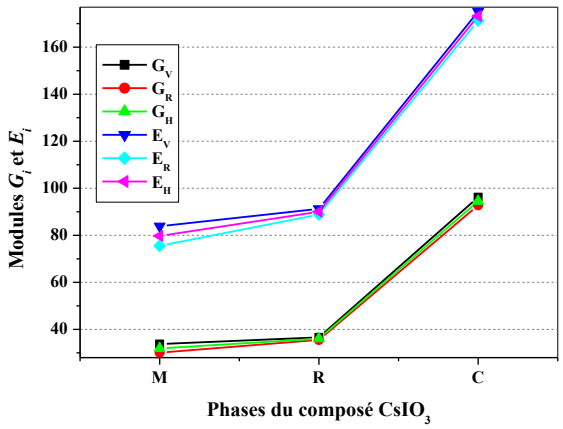


Figure II.6: Relation between Young ***Ei***, and shear ***Gi*** moduli for phases M, R, and C of $CsIO_3$.

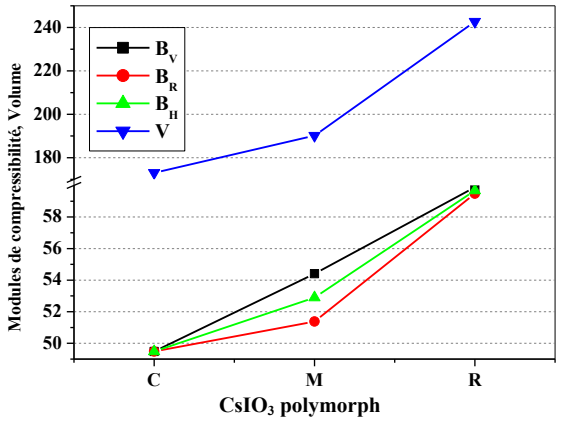


Figure II.7: Relation between compression ***Bi*** modulii and volume **V** with phases M, R, and C of $CsIO_3$.

We observe that the values obtained for ***Bi***, ***Gi***, and ***Ei*** (***i* = *V*, *R*,** or ***H***) for the three monovalent cesium iodates are close to each other, but those for C-$CsIO_3$ are relatively the largest.

We also note that:

- The values of the compressive moduli B_i ($i = R, V$, or H) indicate that R-$CsIO_3$ is the hardest (compressible) and C-$CsIO_3$ the softest (compressible).
- The shear moduli G_i ($i = R$, V, or H) demonstrate that C-$CsIO_3$ the higher resistance to plastic deformation.
- The Young's moduli E_i ($i = R$, V, or H) also indicate that M-$CsIO_3$ is the least rigid in its series, while C-$CsIO_3$ is the most rigid.

We can clearly see from this figure that all our iodates are more ductile than compressible than shear-resistant ($Ei > Bi > Gi$).

This correlation is linked to the lattice parameter **a**, where the ***Gi*** and ***Ei*** moduli are proportional.

The ***B/G*** ratio is used to determine whether the compound is ductile or brittle. For this purpose, the Pugh criteria [26] are used. According to these criteria, a compound is:

- **Ductile:** when $B/G > 1.75$.
- **Brittle:** if $B/G < 1.75$.

Therefore, the three iodates are characterized by brittle behavior.

The ***B/G*** ratio of **1.66** is the highest value assigned to M-$CsIO_3$, indicating that this material is more ductile than the two others.

Another criterion for ductility and brittleness is Poisson's ratio σ ($0 < \sigma < 0.5$) such that [24]:

- $\sigma > 0.26$, the material is **ductile.**
- $\sigma < 0.26$, the material behaves **brittle.**

The three $CsIO_3$ polymorphs are then characterized by a **brittle** behavior.

These findings are in good agreement with the ***B/G*** criteria.

Another meaning attributed to Poisson's ratio σ is the nature of the bonds in the material. From weak (Van der Waals) bonds, through medium-strength (covalent) bonds, to strong (ionic) bonds, the value of σ increases.

Regarding the nature of the bonds, we have [27]:

- $\sigma \geq 0.1$, the material is covalent.
- $\sigma \geq 0.25$, the material is ionic.

Our obtained Poisson's ratio values are between 0.249 and -0.083, which indicates that our materials exhibit covalent-fairly ionic character.

Despite the fluctuations in the hardness, plastic deformation, and stiffness rankings, it is clear from our results that the parameters ***B/G*** and σ have values inversely proportional to the symmetry degree of the iodate phase.

This observation should be taken into account given that the three systems are polymorphs. To generalize this rule, it is necessary to broaden the study to systems of different classes in order to assess the effect of structural changes on these parameters and even on other parameters characterizing solid states.

II.4.3. Elastic anisotropy

Elastic anisotropy is a directional property; it is the response of a material in different directions when it is subjected to stresses. It is expressed by an international (or universal) anisotropy index symbolized by $\boldsymbol{A^U}$.

Equation (II.44) allows the calculation of this index [28]:

$$A^U = 5\frac{G_V}{G_R} + \frac{B_V}{B_R} - 6 \geq 0 \qquad \text{II.44}$$

We calculated the international (or universal) anisotropy index $\boldsymbol{A^U}$, and the results are reported in table II.8.

It is clear that all the $\boldsymbol{A^U}$ values are positive, but M-$CsIO_3$ has the highest value.

We note that the values are all positive, therefore our materials are all anisotropic. R-$CsIO_3$ and C-$CsIO_3$ are less elastically anisotropic than M-$CsIO_3$, and the latter is considered the most elastically anisotropic.

We evidently conclude that our phases are all anisotropic (positive values of A^U) and that M-$CsIO_3$ is the most anisotropic followed by C and R (the two later having close values).

Table II.8: Elastic anisotropy A^U for phases M, R, and C of $CsIO_3$.

Material	M-$CsIO_3$	R-$CsIO_3$	C-$CsIO_3$
A^U	0.6655	0.1616	0.1848

To more illustrate the elastic anisotropic character of the studied structures, we plotted the bulk modulus *B* and the Young's modulus *E* in two dimensions (2-D) and three dimensions (3-D). Figures from II.8 to II.13 demonstrate the obtained plots for M, R and C phases respectively.

A more in-depth discussion of the results is provided for each compound separately (below each figure).

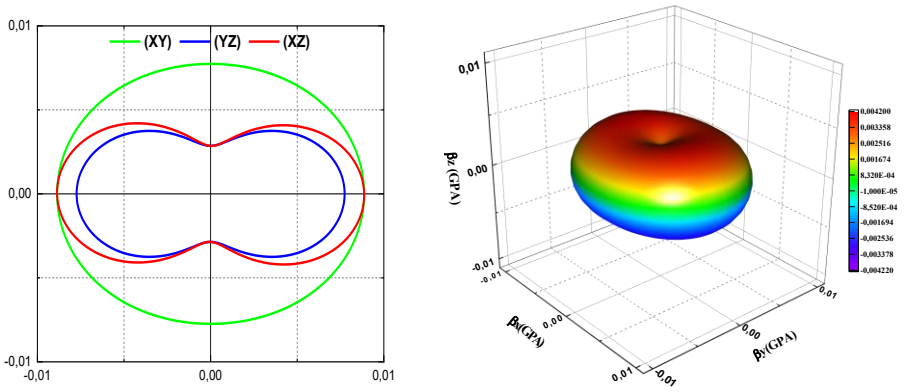


Figure II.8: Bulk modulus *B* of the M-$CsIO_3$ in 2-D (left) and 3-D (right).

- Compression along the xy axis is significantly greater than that along the xz axis, and along the latter is greater than yz axis.
- The 3D geometric shape is significantly deviated from sphericity, giving M-$CsIO_3$ a substantial anisotropy.

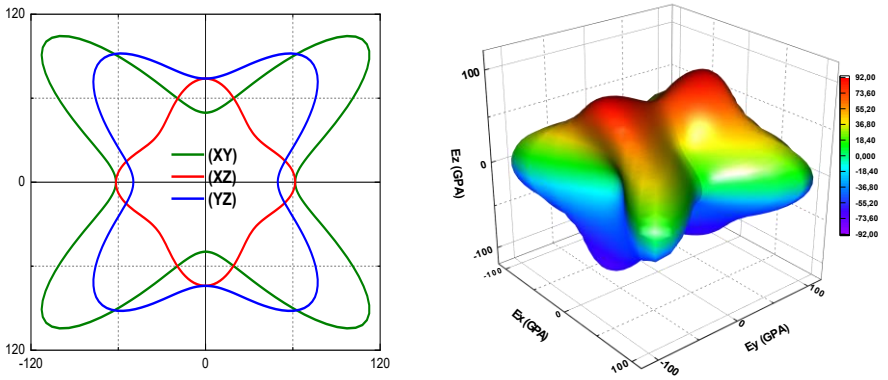


Figure II.9: Young modulus *E* of the M-$CsIO_3$ in 2-D (left) and 3-D (right).

- For E_i, the projection is not spherical.
- The deviation from sphericity is identical along (xz) and (yz) and greater than that along (xy).
- M-$CsIO_3$ is an elastically anisotropic compound.

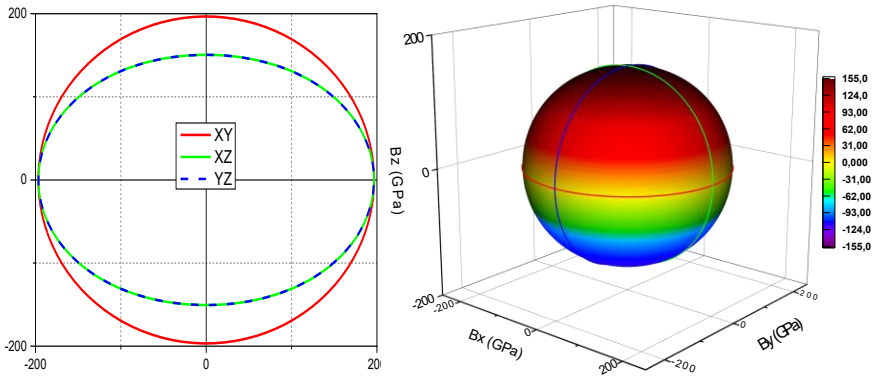


Figure II.10: Bulk modulus B of the R-$CsIO_3$ in 2-D (left) and 3-D (right).

- R-$CsIO_3$ is more compressible along the (xy) axis.
- Its compressions along the (xz) and (yz) axes are identical.
- The anisotropy in all three directions is similar.
- There is some deviation from sphericity, but it is much less significant than in the other three materials.
- The anisotropy along (xz) and (yz) is more pronounced compared to (xy).

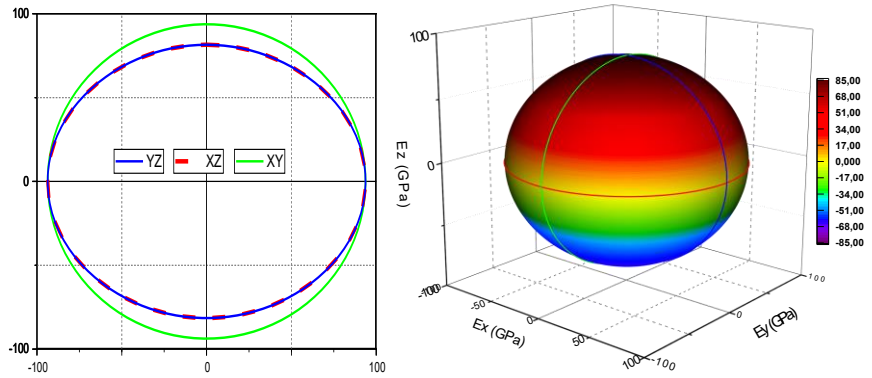


Figure 11: Young's modulus E of the R-$CsIO_3$ in 2-D (left) and 3-D (right).

- R-$CsIO_3$ is stiffer along the (xy) axis.
- The stiffness along the (xz) and (yz) axes is identical.

- Slight deviations from sphericity are observed along all three axes, but these are less pronounced along the xy axis.
- A weak anisotropy for R-$CsIO_3$ is observed.

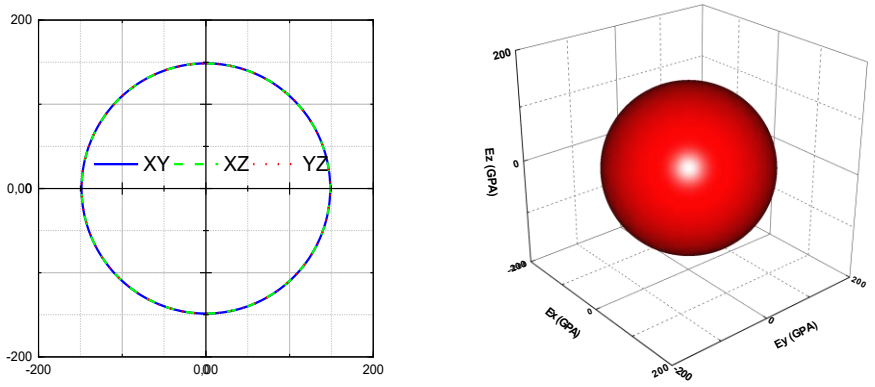


Figure 12: Bulk modulus *B* of the C-$CsIO_3$ in 2-D (left) and 3-D (right).

- Figure II.12 clearly illustrates the isotropic compressibility of C-$CsIO_3$.
- C-$CsIO_3$ has similar rigidity along the three axis.
- It is identically rigid along (xz), (xy), and (yz).
- Its deviation from sphericity (anisotropy) is zeroed compared to that of R-$CsIO_3$ and M-$CsIO_3$.

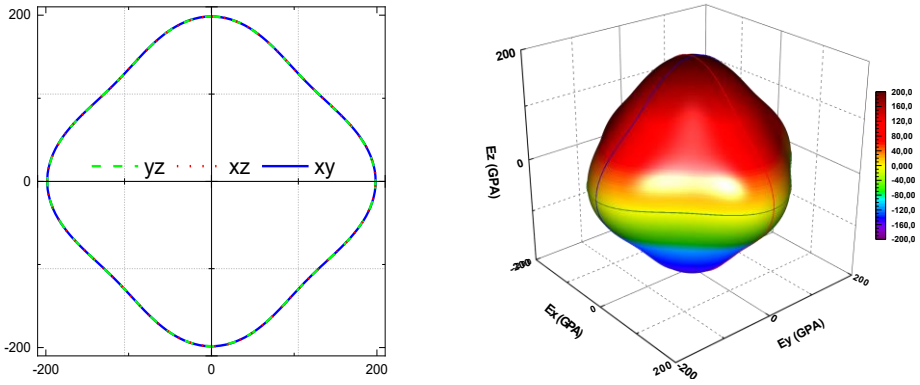


Figure II.13: Young modulus *E* of the C-$CsIO_3$ in 2-D (left) and 3-D (right).

- This phase is clearly isotopic because it exhibits identical shear patterns along the three axes YZ, XZ and XY.
- Initial analysis of E_i patterns shows that the surfaces are symmetrical but not spherical. They exhibit significant deviations from sphericity, indicating that our material is anisotropic and has extents that differ from one iodate to another.

In conclusion, we can say:

According to figures II.8 and II.9, the monoclinic cesium iodate M-$CsIO_3$ clearly shows enhanced elastic anisotropy in the three directions (important deviation from sphericity with both bulk and Young moduli).

For R structure, there is some deviation from spherical shape with both moduli but less important in (xy) direction (figures II.10 and II.11).

The cubic phase is obviously isotopic according to bulk plots (figure II.12) but from figure II.13 it is clearly anisotropic and with an identical behaviour in the three directions (xy, xz and yz).

In the next sections, cubic cesium iodate is not considered since it is centrosymmetric and doesn't own piezoelectric and nonlinear optical (NLO) properties.

II.5. Piezoelectric properties

The iodate compounds subject of this work (M, and R) have several independent piezoelectric coefficients ***dij*** and their distribution in the tensor is detailed in the matrix presented in equations II.45 and II.46 below respectively **[19,20,22]**.

For the M phase:

$$\begin{bmatrix} d_{11} & d_{12} & d_{13} & 0 & d_{15} & d_{16} \\ 0 & 0 & 0 & d_{24} & 0 & d_{26} \\ d_{31} & d_{32} & d_{33} & 0 & d_{35} & 0 \end{bmatrix} \quad \text{II.45}$$

For the R phase:

$$\begin{bmatrix} 0 & 0 & 0 & 0 & d_{15} & -2d_{22} \\ -d_{22} & d_{22} & 0 & d_{15} & 0 & 0 \\ d_{31} & d_{31} & d_{33} & 0 & 0 & 0 \end{bmatrix} \quad \text{II.46}$$

The calculation of the piezoelectric coefficients resulted in the results reported in table II.9.

From a general inspection of the results, the monoclinic compound M acquires larger coefficients but d_{31} and d_{33} are greater with R-phase.

Table II.9. Piezoelectric coefficients d_{ij} (pc/N) calculated for M-$CsIO_3$ and R-$CsIO_3$.

Phase	**Piezoelectric coefficient d_{ij} (pc/N)**										
M	d_{11}	d_{12}	d_{13}	d_{15}	d_{16}	d_{24}	d_{26}	d_{31}	d_{32}	d_{33}	d_{35}
	15.2	16.9	-12.1	-0.24	9E-5	-0.06	37.74	-0.03	-9E-3	-0.03	1.99
R	d_{15}			d_{22}			d_{31}			d_{33}	
	-32.06			-42E-7			-4.27			-8.16	

The maximum values are $|d_{15}|$=32.06 (for R) and d_{26}=37.74 (for M) which are close to each other. This is possibly due to the pseudo-rhombohedric structure of the M-phase with a≈b≠c and β=90.8°≈90°. In conclusion, more the material is structurally symmetric less it has important piezoelectricity. Finally, we can say that M-$CsIO_3$ is more piezoelectric.

We observe that the values of the ***dij*** coefficients of the R-$CsIO_3$ compound are the most significant, with the exception of d_{22}, which are almost zero for all.

We also note that d_{15} is the most significant value for R-$CsIO_3$ compound and d_{26} for M-$CsIO_3$.

II.6. Nonlinear optical properties (ONL)

NLO properties reported in this section are electrooptic coefficients r_{ij} and second order optical coefficients $\mathbf{d_{ij}}$.

II.6.1. Electro-optical coefficients

M-$CsIO_3$ has ten independent electro-optic coefficients as follows [29]:

$$\begin{bmatrix} r_{11} & 0 & r_{13} \\ r_{21} & 0 & r_{23} \\ r_{31} & 0 & r_{33} \\ 0 & r_{42} & 0 \\ r_{51} & 0 & r_{53} \\ 0 & r_{62} & 0 \end{bmatrix} \qquad \text{II.47}$$

R-$CsIO_3$ crystallizes in the 3m class, thus possessing four independent electro-optical coefficients ***rij*** (r_{11}, r_{13}, r_{33} et r_{51}). Their tensor form is illustrated in equation (II.48) [29].

$$\begin{bmatrix} r_{11} & 0 & r_{13} \\ -r_{11} & 0 & r_{13} \\ 0 & 0 & r_{33} \\ 0 & r_{51} & 0 \\ r_{51} & 0 & 0 \\ 0 & -r_{11} & 0 \end{bmatrix} \qquad \text{II.48}$$

The calculated values of r_{ij} (pm/V) obtained for both materials are shown in table II.10.

Table II.10: Calculated electro-optic coefficients r_{ij} (pc/N) of monoclinic and rhombohedric cesium iodates.

Phase	**Electrooptic coefficients r_{ij} (pc/N)**									
M	r_{11}	r_{13}	r_{21}	r_{23}	r_{31}	r_{33}	r_{42}	r_{51}	r_{53}	r_{62}
	12.93	0.03	10.09	0.03	-0.06	-0.16	-12E-5	-85E-4	0.23	11.23
R	r_{11}		r_{13}			r_{33}			r_{51}	
	-5.56		-8.40			-11.48			-10.14	

Both systems have comparable values of r_{ij}, nevertheless those important with R phase are neglected with M phase (around zero) except for r_{11}.

Maximum values are r_{11}=12.93 for M and $|r_{33}|$=11.48 for R indicating that the former is slightly more electro-optic than the later considering the pseudo-rhombohedric structure of M.

It is clear from these results that R iodate has the most important electro-optical coefficients.

The calculated ***rij*** coefficients for the M and R phases of CsIO3 are similar in magnitude, but those which are important in the M phase are found negligible in the other R phase and vice versa.

The highest value between the two phases, r_{11} = 12.93, is attributed to the M phase.

For the **R** phase, its highest value is r_{33} = 11.48 which is not far from that of the M phase. This can also be explained by the pseudo-rhombohedral structure of the monoclinic M phase.

II.6.2. Second-order optical coefficients

The exploited $CsIO_3$s materials possess ten and three second-order optical coefficients for M and R phases respectively, which are represented in the following tensor form [30]:

$$\begin{bmatrix} d_{11} & d_{12} & d_{13} & 0 & d_{15} & 0 \\ 0 & 0 & 0 & d_{24} & 0 & d_{26} \\ d_{31} & d_{32} & d_{33} & 0 & d_{35} & 0 \end{bmatrix} \quad \text{II.49}$$

$$\begin{bmatrix} 0 & 0 & 0 & 0 & d_{31} & -d_{22} \\ -d_{22} & d_{22} & 0 & -d_{22} & 0 & 0 \\ d_{31} & d_{31} & d_{33} & 0 & 0 & 0 \end{bmatrix} \quad \text{II.50}$$

The results obtained are reported in table II.11.

Table II.11. Second order optical coefficients d_{ij} calculated for M and R polymorphs of $CsIO_3$.

Phase	**Second order coefficient d_{ij} (pm/V)**									
M	**d_{11}**	**d_{12}**	**d_{13}**	**d_{15}**	**d_{24}**	**d_{26}**	**d_{31}**	**d_{32}**	**d_{33}**	**d_{35}**
	-19.32	-14.17	-3.05	0.031	-0.087	-14.17	0.031	-0.087	-0.31	-3.05
R	**d_{22}**			**d_{31}**				**d_{33}**		
	0.00			14.06				16.83		

As already reported for the electro-optical coefficients ***rij***, the second-order optical coefficients dij show a maximum value d_{11} = 19.32 (by analogy with r_{11}) attributed to the M phase.

The highest value of the **R** phase is d_{33} = 16.83 (by analogy with r_{33}). The two values are close to each other.

The **dij** values are encouraging and significantly higher than those of some chalcopyrite compounds [31]. Those of M-$CsIO_3$ are the most enriched, which suggests a much better ONL functionality.

The **d_{22}** values are all zero, which is favorable for GSH. Comparing the **d_{31}** values, we conclude that the increasing degree of GSH functionality is as follows: R-$CsIO_3$, M-$CsIO_3$.

We note that **d_{33}** is the largest for R iodate where **d_{31}** is the largest for the M phase.

M and R phases present maximum grades at $|d_{11}|$=19.32 (by analogy with r_{11} as maximum value) and d_{33}=16.83 (by analogy with r_{33} as maximum) respectively showing up that the monoclinic polymorph exhibit somewhat a better second order optical character than the rhombohedric polymorph (taking into account the pseudo-rhombohedric structure of the M phase).

II.7. Conclusion

The aim of the present work is the theoretical investigation of structural, electronic, mechanical and optical properties of three cesium iodate $CsIO_3$ polymorphs; monoclinic (M), rhombohedric (R) and cubic (C) by means of density functional theory (DFT). The calculated structural parameters by the two methods (GGA and LDA) are in good agreement with experimental ones especially those obtained with GGA method (with some exceptions).
Most considered properties are intrinsically related to the difference in structure from one polymorph to another. Monoclinic system M-$CsIO_3$ displays higher birefringence, Poisson ratio σ, B/G ratio and elastic anisotropy, and also better piezoelectric and nonlinear optical properties while its cubic structure (C) has enhanced resistance toward compression and toward shear and elevated values of shear G_i and Young E_i moduli. In the case of R-$CsIO_3$, it has superior band gap value (C phase having metallic characteristic), higher bulk modulus B_i, but in particular, its piezoelectric and nonlinear optical tendencies are less but close to those found for monoclinic $CsIO_3$ which is explained by the pseudo-rhombohedral structure of the later. In conclusion, M-$CsIO_3$ is a better mechanical, nonlinear, and piezoelectric functional material while R-$CsIO_3$ is a better electro-optic functional material.

In order to highlight structure-property relationships for iodate compounds, the three polymorphs were analyzed. The study of the different properties of the monoclinic, rhombohedral, and cubic phases of the compound $CsIO_3$ allowed us to draw the following conclusions:

- The values of the ***B/G*** ratio and Poisson's ratio σ are inversely proportional to the symmetry degree of the three phases.
- All other mechanical properties indicate that M and R materials are anisotropic while the C phase is mostly isotropic, this is confirmed by the NCS of the two former and the CS of the latter.

The various properties calculated for the three monovalent iodates are very encouraging with regard to the intended applications for these materials. In this series, R-$CsIO_3$ exhibits the best functionality, especially in nonlinear optics (NLO).

In general, the M phase has slightly larger piezoelectric coefficients than the R phase, but d_{31} and d_{33} are more significant in the R phase.

The maximum value for compound R is d_{15} = -32.06, and for the M phase it is d_{26} = 37.74, which is close to that of R.

This can be explained by the fact that the M phase is characterized by a pseudo-rhombohedral structure, since its lattice parameters are very close to a rhombohedral structure with a, b, c, and $\beta = 90.8°$.

This may mean that the more symmetrical a material is, the lower its piezoelectricity.

References

[1]: X. Gonze; J.-M. Beuken; R. Caracas; F. Detraux; M. Fuchs; G.-M. Rignanese; L. Sindic; M. Verstraete; G. Zerah; F. Jollet; M. Torrent; A. Roy; M. Mikami; Ph. Ghosez; J.-Y. Raty; D.C. Allan, Computational Materials Science, 25 (2002) 478.

[2]: C. G. Wang, *Acta Chim. Sinica* **43** (1985) 271.

[3]: M. Zhang, C. Hu, T. Abdudouwufu, Z. Yang, S. Pan, Chem. Mater. 30 (2018) 1136.

[4]: W. H. Zachariasen, *Skrifter utgitt av det Norse Videnskaps-Akademi I Oslo 1: Matematisk-Naturvidenskapelig Klasse* 1928 (1928) 1.

[5]: J. P. Perdew, Y. Wang. Phys. Rev. B 45, 13244 (1992).

[6]: N. Troullier, J. L. Martins. Phys. Rev. B 43, (1991) 1993.

[7]: M. Fuchs, M. Scheffler, Computer Physics Communications 119 (1999) 67.

[8]: S. Baroni, S. de Gironcoli, A. Dal Corso, and P. Giannozzi. Rev. Mod. Phys. 73, (2001) 515.

[9]: H. B. Schlegel. J. Comp. Chem. 3. 214 (1982).

[10]: E. Coquet, J. M. Crettez, J. Pannetier, J. Bouillot and J. C. Damien, Acta Cryst. B 39, (1983) 408.

[11]: N. W. Alcock, Acta Cryst. B 28 (1972) 2783.

[12]: K. Momma, F. Izumi, J. Appl. Cryst. 44 (2011) 1272: VESTA (Visualization for electronic and structural analysis) Ver. 3.4.2. (2017).

[13]: H. L. Wheeler, S.I. Penfield, *Z. Anorg. Chem.* 2 (1892) 437.

[14]: T. V. Barker, Note on the iodates and periodtes of the alkali metals and the ammonium radical XCIII (1902) 15.

[15]: A. F. Armington, J. J. O'Connor, Mat. Res. Bull. 6 (1971) 635.

[16]: T. G. Balicheva, G. A. Petrova, Zhurnal Strukturnoi Khimii 14(3) 463.

[17]: C-L. Hu, J-G. Mao, *J. Phys.: Condens. Matter.* 22 (2010) 155801.

[18]: A. H. Reshak, O. V. Parasyuk, H. Kamarudin, I. V. Kityk, Z. A. Alahmed, N. S. AlZayed, S. Auluck, A. O. Fedorchuk, J. Chysky, RSC Adv., 2016. DOI: 10.1039/C6RA12734G.

[19]: R. F. Tinder. "Tensor Properties of Solids" synthesis lectures on engineering 4 Morgan and Claypool Publishers (2008).

[20]: F. Mouhat, F-X. Couder. Phys Rev B 90. 224104 (2014).

[21]: Z-J. Wu, E-J. Zhao, H-P. Xiang, X-F. Hao, X-J. Liu. J. Meng. Phys. Rev. B 76, 054115 (2007).

[22]: R. E. Newnham, Properties of materials: Anisotropie, Symmetry, Structure, Oxford University Press Inc., New York (2005).

[23]: W. Voigt, Lehrbuch der Kristallphysik, Teubner, Leipzig, (1928).

[24]: A. Reuss, Z. Angew. Math. Mech. 9, 49 (1929).

[25]: R. Hill, Proc. Phys. Soc. London A 65,349 (1952).

[26]: Pugh Pugh, S. F. Philos. Mag. 1954, 45, 823-843.

[27]: I. R. Shein, A. L. Ivanovskii, Scripta Materiaia 59 (2008) 1099.

[28]: S. I. Ranganathan, M. Ostoja-Starzewski, Physical Review Letters 101 (2008) 055504-1.

[29]: A. Authier, "International Tables for Crystallographie, volume D: Physical Properties of Crystals", Kluwer Academic Publishrs (2003).

[30]: R. C. Powell, Symmetry, Group Theory and the Physical Properties of Crystals, Springer Science and Business Media, LLC. (2010).

[31]: T. Dahame, Thèse de Doctorat, Université de Laghouat-Algérie (2016)

General conclusion

General conclusion

In this work, a theoretical investigation of the structural, mechanical, piezoelectric, and nonlinear optical properties of cesium iodate ($CsIO_3$) polymorphs has been carried out using first-principles calculations based on Density Functional Theory (DFT).

The considered polymorphs are the monoclinic (M-$CsIO_3$), the rhombohedral (R-$CsIO_3$), and the cubic (C-$CsIO_3$) forms.

The obtained results show that the crystal structure has a significant influence on the physical properties of the studied phases. The monoclinic and rhombohedral polymorphs were found to be mechanically stable, whereas the cubic phase exhibits mechanical instability. The calculated elastic parameters reveal anisotropic behavior and indicate that the studied stable phases possess a brittle character.

Furthermore, the piezoelectric and nonlinear optical calculations demonstrate that the non-centrosymmetric phases (M and R) exhibit promising responses, making them attractive candidates for optical, electro-optic, and photonic applications. These findings highlight the strong relationship between crystal symmetry and the resulting functional properties of $CsIO_3$ polymorphs.

Overall, this study contributes to a better understanding of cesium iodate polymorphs and provides useful theoretical data for future experimental and theoretical investigations. The obtained results suggest that $CsIO_3$-based materials may represent promising candidates for advanced nonlinear optical and optoelectronic devices.

عنوان المذكرة: دراسة نظرية للخواص البنيوية والميكانيكية والبصرية غير الخطية لأشكال متعددة من أيودات السيزيوم

اللقب: معيزي **الإسم**: عبد الجليل **المؤطرة**: د. بلحاج صوراية

ملخص:

تتناول هذه الدراسة الخواص البنيوية والميكانيكية والبصرية اللاخطية لمتعددات الأشكال لمركب يودات السيزيوم ($CsIO_3$)باستخدام نظرية الكثافة الوظيفية (DFT). أظهرت النتائج أن الطورين أحادي الميل والرومبوهدري مستقران ميكانيكياً، بينما الطور المكعب غير مستقر. كما كشفت الدراسة عن خواص بصرية لاخطية وكهروضغطية واعدة، مما يجعل هذا المركب مناسباً للتطبيقات البصرية المتقدمة.

كلمات مفتاحية: $CsIO_3$، الأشكال المتعددة، نظرية الكثافة الوظيفية، الخواص الميكانيكية، البصريات غير الخطية.

Memory title: **Theoretical investigation of the structural, mechanical, and nonlinear optical properties of cesium iodate polymorphs**

Name: MAIZI **First name:** Abdeljalil **Directed by:** Dr. S. BELHADJ

Abstract:

This work investigates the structural, mechanical, and nonlinear optical properties of cesium iodate ($CsIO_3$) polymorphs using Density Functional Theory (DFT). The results show that the monoclinic and rhombohedral phases are mechanically stable, whereas the cubic phase is unstable. Significant piezoelectric and nonlinear optical responses were obtained, highlighting the potential of $CsIO_3$ for advanced optical and photonic applications.

Key words: $CsIO_3$, Polymorphs, DFT, Mechanical properties, Nonlinear optics.

Titre du mémoire: **Étude théorique des propriétés structurales, mécaniques et optiques non linéaires des polymorphes de l'iodate de césium**

Nom: MAIZI **Prénom:** Abdeljalil **Encadreur:** Dr. S. BELHADJ

Résumé:

Cette étude porte sur les propriétés structurales, mécaniques et optiques non linéaires des polymorphes de l'iodate de césium ($CsIO_3$) à l'aide de la théorie de la fonctionnelle de la densité (DFT). Les résultats montrent que les phases monoclinique et rhomboédrique sont mécaniquement stables, tandis que la phase cubique est instable. Les propriétés piézoélectriques et optiques non linéaires obtenues révèlent un potentiel intéressant pour les applications optiques avancées.

Mots clés: $CsIO_3$, Polymorphes, DFT, Propriétés mécaniques, Optique non linéaire.